Lawrence Berkeley Laboratory
UNIVERSITY OF CALIFORNIA

Accelerator & Fusion
Research Division

Submitted to Review of Scientific Instruments

DOPPLER SHIFT SPECTROSCOPY OF POWERFUL NEUTRAL BEAMS

C. F. Burrell, W. S. Cooper, R. R. Smith, and W. F. Steele

April 1980

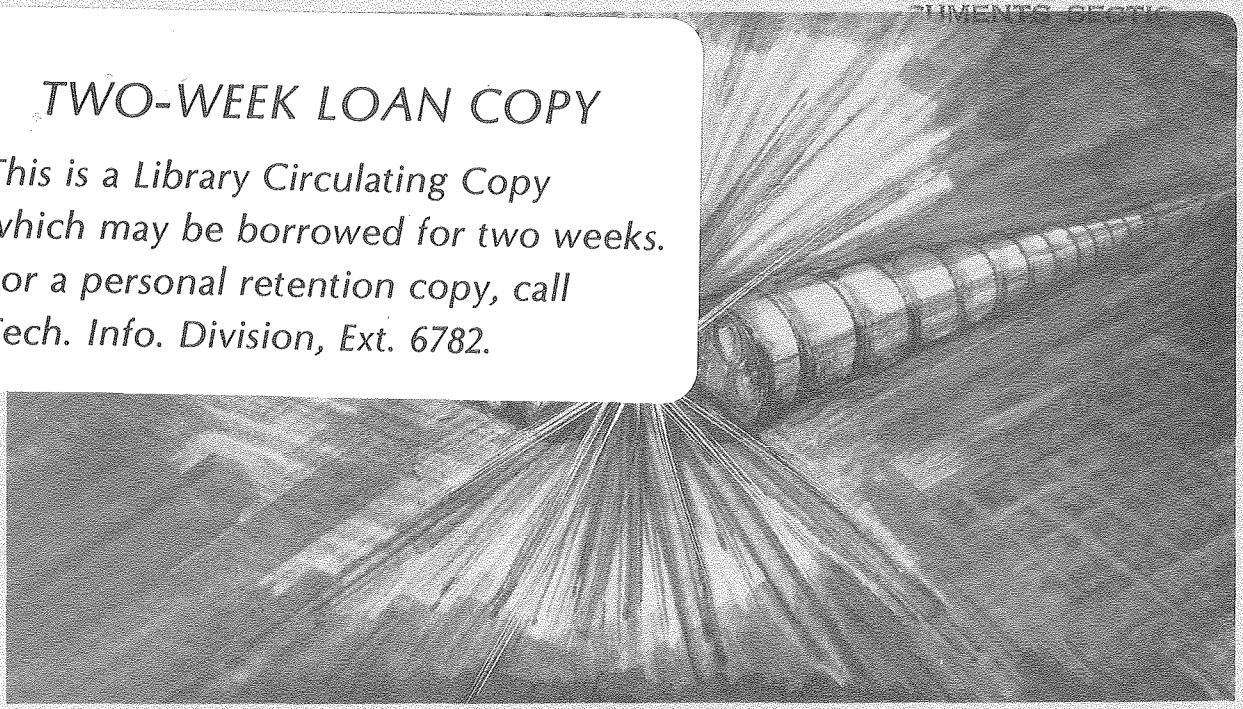

Prepared for the U.S. Department of Energy under Contract W-7405-ENG-48

DISCLAIMER

Doppler Shift Spectroscopy of Powerful Neutral Beams*

C. F. Burrell, W. S. Cooper, R. R. Smith, and W. F. Steele

Lawrence Berkeley Laboratory
University of California
Berkeley, California 94720

3. Introduction

The Lawrence Berkeley Laboratory has been conducting research and development for the production of high powered beams of neutral hydrogen and deuterium atoms for several years.[1,2] The power densities frequently exceed 5 kW cm^{-2} and render it difficult to characterize the beam with probes that are inserted into the beam. It is important to measure the spatial distribution of beam power and also the energy distribution of accelerated hydrogen atoms. This energy distribution is influenced by: 1) the proportion of single, double, and triple mass hydrogen ions in the plasma source; 2) charge exchange and dissociation within the accelerator structure; and 3) possible collective effects in the neutralizer which may affect the energy and divergence of ions. We have developed an optical diagnostic which we use to make all the above measurements. The spectrum of H_α or H_β light emitted by fast hydrogen (or deuterium) neutrals is observed along an optic axis at an angle to the neutral beam axis. The light is Doppler shifted sufficiently to resolve easily the three dominant energy components of the neutral beam; accelerated molecular ions H_2^+ and H_3^+ fragment in the neutralizer gas cell and produce neutral atoms at 1/2 and 1/3 of the full energy, as well as full energy neutrals from H^+ ions. On-line computerized data reduction plus the capability of archival storage

*Work supported by U. S. Department of Energy, Office of Fusion Energy, under contract W-7405-ENG-48.
+Permanent address: Princeton Plasma Physics Laboratory, Princeton New Jersey 08544.

allow an unusually thorough analysis. With this non-perturbing technique we have been able to make measurements of the divergence of each energy component of the neutral beams in two planes with a time resolution of about 10 msec if the light is shuttered with a mechanical aperture. Furthermore the different divergences of different energy components, which differ presumably due to the energy of dissociation of the molecular ions, are easily resolved. An analysis of the relative amounts of light from the three components in the beam has produced a measured species distribution emerging from the ion source which agrees within 5% with measurements made by other diagnostics. The presence of an oxygen impurity in the neutral beam can be monitored by observation of a spectral line caused by relatively low energy hydrogen atoms which result from the fragmentation of H_2O^+, HO^+, and H_3O^+ ions accelerated by the source.

We have reported earlier on the measurement of neutral beam divergence[3] and ion species[4] by the method of high resolution spectroscopy employing an optical multichannel analyzer (500 channels) presented in detail in this paper. Ulrickson and Bussac[5] have reported on a spectroscopic measurement of ion species which employs a rapid scan spectrometer. Recently Bonnal et al[6] have reported on spectrographic measurements of ion species which employ optical guides and an array of photomultiplier tubes.

I. Experimental Methods

Light which is emitted from the neutralizer section is collected by a 25 cm focal length lens and is focused on the entrance slit of a Spex Model 1704 1-meter monochromator with a 1800 gr/mm holographic grating.

A system of mirrors provides that the optical system simultaneously views the neutralizer in a plane parallel to the accelerator slots and in a plane perpendicular to the accelerator slots. The optic axis makes an angle of 78^{o} with the neutral beam axis in the parallel plane and an angle of 111^{o} with the neutral beam axis in the perpendicular plane. In the appendix we show that with this arrangement we can measure the beam divergence parallel and perpendicular to the accelerator slots with very little coupling between the measurements. We illustrate in Fig. 1 this small coupling for a particle moving in the x-z plane with an optic axis in the y-z plane. The problem of reflected light from the exit windows was solved by placing the windows at such an angle that the view of the neutral beam as reflected in the exit window is normal to the neutral beam axis and therefore reflected light from fast neutral atoms has a negligible Doppler shift and overlaps only the unshifted line. The monochromator can be rolled on rails to four sets of viewing ports located 33, 62, 129, and 196 cm from the accelerator exit grid.

The spectrum produced by the monochromator is imaged onto a P.A.R. Model 1205A optical multichannel analyzer (O.M.A.) which uses as a detector a vidicon tube with a silicon intensified target (S.I.T.). This system provides a 500 channel analysis of the distribution of emitted light as a function of wavelength. The combination of monochromator and O.M.A. gives a resolution of 0.137 Angstroms per channel. The data which is collected is read out after every shot by a Modular Computer Systems Modcomp II computer where the data is analyzed for real time display or saved on a disk for later analysis.

If the optic axis makes an angle θ with a neutral particle trajectory, then the emitted light is Doppler shifted from a wavelength λ_o in the rest frame, to a wavelength λ in the laboratory frame:

$$\lambda = \frac{(1-\beta \cos \theta)}{\sqrt{1 - \beta^2}} \lambda_o, \quad \beta = v/c \tag{1}$$

where v is the atomic hydrogen velocity which is known from the accelerating voltage. It is important to use a relativistically correct analysis if the aiming direction of the neutral beam (from the Doppler shift of the full energy component) is desired by this technique because the transverse relativistic Doppler shift of the H_α Balmer line of a 120 keV hydrogen beam is 0.8 Å, which is approximately six channels in our O.M.A. system. The transverse velocity distribution of each atomic component determines the width of its spectral line profile; from this information one can calculate the beam divergence of each component.

To assure that we are fully using the light gathering capacity of the monochromator we set the wavelength scale to zero (in order to transmit zero order diffracted light from the grating) and pass white light back through the monochromator, fully illuminating the grating. We then observe that the beam of light emerging from the entrance slit passes unobstructed through the lens and windows of the optical system and that the beam of light passes through the central region of the neutral beam over which the current density is nearly uniform. If these conditions are satisfied the sensitivity of the optical system is independent of the distance between the monochromator and the neutral beam axis. For neutral beams of minimum width, 10 cm (characteristic of the large area sources developed at our laboratory), and a 1-meter monochromator it should be possible to place the monochromator up to 10

meters from the neutral beamline without significant attenuation. Even greater separation may be possible through the use of fiber optics or a series of relay lenses at the cost of some attenuation of the signal.

Instrumental broadening can be caused by five effects: Stark broadening, fine structure, monochromator instrument function, O.M.A. instrument function, and the angular divergence of the light collection optics. The first of these is negligible for our conditions. By observing hydrogen light from a Geisler tube the second through fourth effects were measured and combined in a small effective instrumental width. The Doppler broadening of the hydrogen light from the Geisler tube is approximately 0.06 Å which causes only a 1% change in the observed broadening of neutral beam light having a Gaussian profile with a spectral width of about 0.5 Å. A numerical calculation of the convolution integral of a Gaussian profile with the instrument function shows that the 1/e halfwidth of the convolution is given approximately by the relation $\Delta\lambda_C^2 = \Delta\lambda_G^2 + \Delta\lambda_I^2$ where $\Delta\lambda_G$ and $\Delta\lambda_I$ are the 1/e halfwidths of the Gaussian and the instrument function. The deviation from this relationship is less than 0.02 Å for $\Delta\lambda_G > 0.4$ Å typical of most of our measurements. The collection optics introduces an additional error. The entrance slit to the monochromator has dimensions of 2 mm by 0.025 mm. With a lens of 25 cm focal length we find a limiting instrumental divergence which is equal to 0.003^o when observing parallel to the slots in the accelerator structure and 0.23^o when observing perpendicular to the slots. In the appendix we show that this causes only a small perturbation of our observed profiles and a small correction can be made for it.

It should be stressed that all of the ion sources studied in this paper were unfocused (i.e. the accelerator structure was planar),

typical of the TFTR neutral beam injectors. The analysis of this diagnostic for focused neutral beam injectors with regard to measuring beamlet divergence and focusing properties is significantly different and will be considered elsewhere.

The 500 channels of the O.M.A. are calibrated in wavelength using known lines of neon near the 4861.33 Å H_β and 6532.73 Å H_α lines which we use for our measurements. In Fig. 2 we see the deviation from linearity of the measured wavelength as a function of the channel number. The observed cubic relationship is caused by aberration in the image intensification stage of the S.I.T. vidicon tube and is taken into account in the computer analysis program. We use a fully automated program to make a least squares fit to the positon of the neon lines; a simple algorithm (using only the three central channels of each spectral line) calculates the center of a line to a fraction of a channel. As shown in Fig. 2 we find that the standard deviation of eleven neon lines in the vicinity of H_β is consistently less than 0.2 O.M.A. channels. However, there is a slight variation with time (over several hours of observation) of the fit parameters caused by thermal effects. This time dependence of the wavelength calibration is negligible for the measurement of divergence and species. However, for the accurate measurements of the neutral beam aiming direction it would be desirable to observe a reference spectral lamp shortly before or after the neutral beam shot. If the full energy Doppler shift is measured to an accuracy of 0.2 channels for a 120 keV deuterium beam, for the system parameters reported in the opening paragraphs, the uncertainty in the aiming direction would be 0.03^{o} provided the accelerating voltage is accurately known.

The scheme of the analysis program is shown in Fig. 3. The steps in the data reduction begin with the reading of the data from the O.M.A. console to the Modcomp II computer. Then the sensitivity versus channel number, determined by calibration with a standard lamp, is applied as a correction factor to the data. The most intense peak in the data is located and identified as the unshifted H_α or H_β line. Next, the cubic correction function is used to assign a wavelength to each channel from the multi-channel analyzer. From the measured accelerator potential, the approximate locations of the peaks of the three main Dopplershifted spectral lines are computed. Our analysis assumes that every atom contributing light to one of the spectral lines has the same energy. The Doppler broadening of a spectral line caused by fluctuations in the accelerator voltage or possible collective effects in the neutralizer is minimized by the rather large angle of our optic axes to the neutral beam axis. For each peak the initial values of parameters which will be used to describe the wavelength distribution of light are chosen. For fitting purposes, the light is assumed to be composed of modified Gaussian peaks on top of a constant background. For each peak there are four fitting parameters: amplitude, Doppler shift, e-folding width, and an exponent to which the Gaussian distribution is raised. We have observed empirically that this modified Gaussian profile provides a good fit to the observed spectral line profiles. Using methods such as are described in Ref. 7, we then adjust thirteen parameters iteratively and consistently to obtain the best fit between the measured wavelength distribution and the assumed one. As an additional task the program can be asked to search for Doppler shifted light from atoms at either 1/18 or 1/10 the full beam energy; these

lines correspond to radiation from hydrogen or deuterium atoms from the breakup of H_2O^+ or D_2O^+ respectively.

II. Model for Emitted Light

Since the light is Doppler shifted, it can be absorbed only by atoms in the neutral beam and not by cold gas in the neutralizer. For typical conditions in the neutral beam the optical depth is approximately 10^{-6} ($\tau = \alpha R$ where α is the absorption coefficient and R is the radius of the beam); therefore it is an excellent approximation to assume the radiative transfer is optically thin.

The passage of an intense hydrogen or deuterium beam through the gas of the neutralizer produces a plasma in the neutralizer. Hence Doppler shifted spectral lines can be induced by collisions of projectile particles with electrons and ions of the plasma as well as the molecular hydrogen of the gas in the neutralizer. The following collisional processes can produce fast excited hydrogen (deuterium) atoms in the beam:

Table I

	References	$\sigma_\alpha(120\ keV)_D$ (cm^2)	$R = n\sigma v$
1) $\underline{H} + H_2 \rightarrow \underline{H}^*$	8,9	2.5×10^{-18}	1.
2) $\underline{H}^+ + H_2 \rightarrow \underline{H}^*$	10	6.4×10^{-19}	0.26
3) $\underline{H_2}^+ + H_2 \rightarrow \underline{H}^*$	11	4.3×10^{-18}	1.7
4) $\underline{H_3}^+ + H_2 \rightarrow \underline{H}^*$	11	7.2×10^{-19}	2.9
5) $\underline{H_2} + H_2 \rightarrow \underline{H}^*$			
6) $\underline{H} + e^- \rightarrow \underline{H}^*$	12,13,14	7.0×10^{-18}	0.0028
7) $\underline{H} + H^+ \rightarrow \underline{H}^*$	15	8.7×10^{-18}	0.0035

Negative ions are neglected because they constitute less than 2% of the beam.[16]

We assume molecular flow for the gas in the neutralizer. Guthrie and Wakerling[17] estimate that the flow in a pipe is molecular if $\lambda > D/3$ where λ is the mean free path and D is the smallest linear dimension of the pipe cross section. For typical gas flows in our neutralizers this condition is not always well-satisfied at the ion source end of the neutralizer; typically $\lambda \sim D/3$ within a factor of two at the source. The target thickness can be measured by mass spectrometry[18] from ratios of molecular ion currents to fractional energy ion currents. The target thickness measured in this way agrees reasonably well, (better than $\pm$ 50%) with calculations based on molecular flow. However, the measured target thickness does not increase as rapidly with gas flow as the molecular flow calculations would indicate. Fortunately, the species measurement based on the model we report here is not highly sensitive to target thickness, as will be shown.

The first five reactions involve collisions with the target gas of the neutralizer; the last two processes are interactions with a plasma created by the passage of the beam through the neutralizer. We will show that for the emission of Doppler shifted optical radiation the interaction of the neutral beam with the plasma in the neutralizer can be neglected.

We have measured the plasma density in the neutralizer by placing a swept Langmuir probe[19] in the central region of the beam 1 cm from an exit grid and shadowed by the exit grid to protect the probe from direct impact of the neutral beam. With a 100 keV deuterium neutral beam from a 10 x 10 cm ion source (accelerator current = 7.8 amp, gas

flow = 5 torr l/sec) we find $n_e = 1.1 \times 10^{11} cm^{-3}$ and $kT_e = 5$ eV. From the impedance of the neutralizer and molecular flow we calculate the gas density in the neutralizer at this point is $n_{D_2} = 10^{14} cm^{-3}$. For these typical conditions then, $n_{D_2}/n_e = 1000$.

D. A. Dunn and S. A. Self[20] have calculated the density and potential distribution in a beam generated plasma for a slab geometry. From their analysis we find the ratio of plasma density to beam density to be:

$$\frac{n_e}{n_b} = \frac{\sigma_{ei} n_o V_b^{1/2} d}{.344 (KT_e/e)^{1/2}} \tag{2}$$

where σ_{ei} is the total cross section for production of an electron-ion pair by a beam particle, V_b is the beam voltage, n_o is the gas density, 2d is the beam width and T_e is the electron temperature of the plasma. Rearranging, we have for the ratio of gas density to plasma density:

$$\frac{n_o}{n_e} = \frac{.344 (KTe_e/e)^{1/2}}{\sigma_{ei} n_b V_b^{1/2} d} . \tag{3}$$

Thus, if the current density and hence n_b is held constant, we expect the ratio of gas pressure to plasma density to remain approximately constant as the gas pressure drops along the neutralizer. Of course, we neglect in this model axial diffusion of plasma due to the density gradient in the axial direction. This may be reasonable, however, since the width of the neutralizer is small compared to its length. Calculations of this density ratio under conditions similar to the experimental parameters give $n_o/n_e \sim 1000$; the measured value is in reasonably good agreement with this calculation.

The transition rate for emission of Balmer alpha or beta radiation by projectiles is $R_o = n_o \sigma^{OPT} v$ and $R_{i-e} = n_e \sigma^{OPT} v$ for collisions with neutral gas molecules and plasma ions and electrons; where v is the projectile velocity and σ^{OPT} is the appropriate optical cross section. In Table I we tabulate the cross sections for the emission of Balmer alpha radiation for a 120 keV deuterium beam and the transition rate R in arbitrary units with $n_o/n_e = 1000$ assumed. We find that the production of Balmer radiation by collisions with plasma electrons and ions is negligible compared with collisions with the neutral gas; we therefore neglect the plasma electrons and ions in the analysis.

Finally we use the Corona model[21] for calculating the distribution of excited states in the neutral atomic beam -- i.e. collisional excitation to a level is balanced by radiative decay. This is justified because all collisional de-excitation rates for the n = 3 level under typical neutralizer conditions are small compared to the radiative decay rate.

To calculate the beam species mix from the measured light intensities we start with the numerical solution of Berkner et al.[18] to the problem of charge exchange and dissociation in the neutralizer. The ion and neutral species in the beam which are included in the model for light emission can be divided into three families: 1) H^o and H^+, 2) 1/2 H^o, 1/2 H^+, H_2^o and H_2^+, and 3) 1/3 H^o, 1/3 H^+, 2/3 H_2^o, 2/3 H_2^+, and H_3^+, which given rise to the full, half, and third energy components of the Doppler shifted beam light. We use an index j to refer to the eleven species considered in this model (j = 1, 11). The light intensity of the i^{th} component (i = 1, 2, 3, corresponding to

full, half, and third energy) is proportional to $N(n)_i$ (the population density of the n^{th} level of excited hydrogen atoms with velocity v_i):

$$N(n)_i = \frac{1}{v_i} \sum_j \int_0^z n_0(z-x)\sigma_j(n)J_j(x)\ \exp\left(-\frac{x}{v_i \tau_n}\right)dx$$

where v_i is the velocity of the i^{th} component, z is the distance between the observation point and the exit grid of the source, n_0 is the density of the gas in the neutralizer, $\sigma_j(n)$ is the optical excitation cross section for the j^{th} species in the mixed beam, $J_j(x)$ is the current density of the corresponding species, τ_n is the lifetime of the n^{th} level of hydrogen, and j is summed over those species contributing to the i^{th} component of the beam. The integral above is calculated numerically assuming a linear pressure drop in the neutralizer corresponding to molecular flow. No optical cross section data is available for the dissociative excitation of fast H_2^0 so we have set this cross section to zero. This appears to be not too serious because if the target is thin, H_2^+ will dominate over H_2^0 and if the target is thick, most of the molecules will be dissociated. For the remaining cross sections we use measured cross sections for the emission of Balmer alpha or beta radiation by fast hydrogen atoms. The cross sections used for all ionic species are available in reference 11. The cross section for Balmer alpha emission for the reaction $\underline{H} + H_2 \rightarrow \underline{H}^*$ has been measured only over the energy range from 10 to 35 keV. We use an extrapolation of this cross section data shown in Fig. 4. Since the current density $J_j(x)$ is related to the source current density of H^+, H_2^+, or H_3^+, we can relate the light intensity to the source

currents. Specifically, we calculate a coefficient γ_i which is the ratio of the light intensity of the i^{th} component to the corresponding current of H^+, H_2^+, or H_3^+ at the source, normalized so that $\gamma_1 = 1$. If the light intensities of the three major components of the beam are I_1, I_2, and I_3, then the source currents H^+, H_2^+, and H_3^+ are proportional to I_1/γ_1, I_2/γ_2, and I_3/γ_3 respectively. We will show later that there is a thick target approximation which is very simple and gives results that are close to the more complex model presented here for target thicknesses which are required for beam neutralization.

III. Results

A typical data spectrum for a 95 keV deuterium neutral beam is shown in Fig. 5. There are peaks on both sides of the unshifted line, corresponding to simultaneous observation parallel to the accelerator slots (blue shifted) and perpendicular to the slots (red shifted). The three dominant energy components of the beam (full, half, and third) are easily resolved. The fourth peak on each side (nearest the unshifted line) is caused by slow moving atoms of approximately 1/10 the full energy. We attribute this component to the fragmentation of the molecular ions D_2O^+, DO^+, and possibly D_3O^+ which are produced in the source by an oxygen impurity. The divergence of these slow atoms combined with the instrumental broadening would not permit the resolution of these three separate lines under these conditions. This "impurity" line is found to be strong after the vacuum system has been cycled to atmosphere. As the ion source is operated repeatedly over several days this impurity line becomes weaker.

A computer-generated display of the reduced data (corresponding to the spectrum shown in Fig. 5) is shown in Fig. 6. The analysis of the data parallel to the accelerator slots is displayed in the upper half of the figure and the reduced data corresponding to observation perpendicular to the accelerator slots is in the lower half. The points in the display on the left are experimental O.M.A. data points obtained in a single shot and the curves are computer-generated fits to the data as discussed earlier. The tabulated output on the right is as follows -- "E": The index 1, 2, and 3 refers to the full, half, and third energy components of the neutral beam. "Light/Comp.": "Light" is the light intensity (integrated over the spectral line) of each component of the beam; "Comp" is the species current (D^+, D_2^+, and D_3^+ at the source). Both are expressed as percentages. "Angle:" This is the aiming direction of the neutral beam relative to the nominal optic angles of 78^o and 111^o. "Divergence:" This is the angular 1/e half-width of a particular component of the neutral beam, in degrees. The numbers in parentheses are the estimated uncertainties as determined by the curve fitting sub-routine.

Note that the divergence in both directions of observation is larger for the half and third energy components than for the full energy component by 0.2^o to 0.3^o. This may be due to the dissociation energy of the molecular species. For example the minimum Frank-Condon dissociation energy of D_2 is 4.5 eV or 2.25 eV/atom. This transverse energy compared to the beam energy of 95 keV implies a divergence of 0.3^o which is of the correct magnitude. The species ratios as measured in the two different directions are in reasonable agreement. The aiming direction of the neutral beam as determined from the Doppler shift of each spectral line differ by less than 0.2^o. The wavelength calibra-

tion is based on stored information in the computer except that the lowest order term in the cubic equation is adjusted in order to correctly predict the position of the unshifted line for each shot. Therefore, due to drift in the higher order terms of the cubic equation for wavelength calibration, the differences in angle may not be significant; however, there may be phenomena such as slight energy losses for beam particles passing through the neutralizer plasma which cause small deviations of the particle energies from the anticipated values, which would in this analysis appear as slight angular deflections.

We also measure the divergence of the beam by a calorimeter instrumented with an array of thermistors.[21] A bi-Gaussian function is fitted to the distribution of the change in temperature as measured by the thermistors. The output of the fitting program yields the equivalent point source angular divergence. We compare in Fig. 7 the spectroscopic and calorimetric measures of the beam divergence perpendicular to the slots as the beam current is varied to find the minimum divergence. They are in reasonable agreement; the full energy divergence determined spectroscopically is somewhat less than the calorimetric divergence and the fractional energy divergences are larger as we would expect since the calorimeter gives a weighted average.

By moving the spectrometer on rails parallel to the neutralizer we are able to observe beam divergence at several points along the neutralizer. The result of measuring divergence as a function of position in the neutralizer is shown in Fig. 8 for a 115 keV hydrogen beam. We find that the divergence of the full energy component appears to increase as the beam traverses the neutralizer; the greatest increase occurs in the first 80 cm. This is not caused by collision with target gas molecules in the neutralizer -- as measurements by A. B. Wittkower et al.[22]

indicate, collisions with target gas molecules increase the divergence of neutral atoms in the beam by less than 0.04^{o} for a 55 keV hydrogen beam passing through a hydrogen gas cell of target thickness $1.4 \times 10^{16} cm^{-2}$. We feel that this may be caused by an instability in the ion beam-plasma system. It is not clear why the 1/2 and 1/3 energy beams do not show the same behavior.

In making these measurements we found that as the accelerating voltage approached 120 keV for a hydrogen beam and observations were made toward the entrance of the neutralizer the spectrum in the vicinity of the H_β line became cluttered with molecular hydrogen lines. This is not too surprising since at high energies, and in particular for the part of the neutralizer close to the source, the dominant species in the beam is H^+. The cross section for the emission of Balmer radiation from the decay of fast hydrogen atoms resulting from the electron capture from molecular hydrogen by the incident protons falls off rapidly at high energies.[10] In addition, at the higher gas densities close to the accelerator the ratio of the plasma density to the beam density can become rather large (experimentally we measure $n_e/n_b \sim 30$ near the exit grid of the accelerator). Thus excitation of the molecular gas (both the molecular lines and the unshifted Balmer lines) may be dominated by electron impact in the region near the ion source. The spectrum was much cleaner with respect to molecular lines in the vicinity of the H_α line and consequently the signal to noise ratio was improved. For these reasons, in application of this technique to very high energy hydrogen neutral beams, we recommend the H_α line rather than H_β.

The species mix of a variety of 10 x 10 cm neutral beam sources has been measured both spectroscopically and by mass spectrometry at numerous

different energies and different gas flows. The mass spectrometer[18] consisted of a hole in the calorimeter beam dump followed by a transverse magnetic field and an array of Faraday cups. By observing ratios of ion currents such as that of D_2^+ to half-energy D^+, the target thickness can be determined, and from this the species mix at the source can be determined. For the spectroscopic data reduction the target thickness was estimated from the gas flow and the impedance of the neutralizer. The spectroscopy thus also measured the species mix at the source. When the spectroscopic analysis for species was applied to both Balmer alpha and Balmer beta emission under identical conditions they gave results that agreed to within one or two percent. The spectroscopic and mass spectrometry measurements of species generally agreed to within 5%. Typical results for the spectroscopic and mass spectrometry methods are shown in Fig. 9.

Normally we integrate the light intensities over the entire pulse duration; however, time resolution can be achieved with this optical technique by either shuttering the light (or the gain of the image intensifier of the S.I.T.) or relying on the 32 msec scan time of the vidicon tube. We use the latter method to obtain the time resolved measurement of species and the water "impurity" line shown in Fig. 10. The time resolution is approximately 150 msec because it takes several scans of the electron beam to recharge the diodes of the vidicon tube. This was a 110 keV deuterium neutral beam operated with a pulse duration of 1.5 seconds. It appears that there is some excessive heating late in the pulse which is causing the outgassing of an oxygen impurity. With the increased oxygen impurity there was also an increase in the beam composition to 90% D^+.

The results presented up to this point were obtained on a high voltage neutral beam line designed for sources with a 10 x 10 cm accelerator cross-sectional area and long pulse operation (1.5 sec). We recently had the opportunity to compare this spectroscopic technique with momentum analysis (mass spectrometry) on a neutral beam line designed for larger sources but limited by power supplies to short pulse durations (23 msec at 120 kev). The tests were somewhat unusual in that they covered a rather large parameter space. The ion source was of the "magnetic bucket" type[23] with an accelerator area of 10 x 40 cm and had internal dimensions of 23 cm x 53 cm by 24 cm deep.

The experimental arrangement of the Doppler shift spectroscopy was similar to that described earlier except that the neutral beam was observed only in plane perpendicular to the accelerator grids (across the 40 cm width of the source) along an optic axis making an angle of 60^{o} with the neutral beam axis. A second difference is that we used a P.A.R. O.M.A. 2 system (including a model 1215 console, a model 1216 detector controller, and a model 1254 S.I.T. detector head). This system was not interfaced with a mini-computer. We stored the shot data on the floppy disk memory of the console and analyzed it later.

The three major peaks of the Doppler shifted D_{α} light (all shots were for a deuterium beam) were well-resolved. The light intensity of each peak was obtained by summing the number of counts in each peak and correcting both for the variation of sensitivity across the vidicon tube and for the nearby continuum. The 1/e half angle divergence of the full energy component was obtained by a linear interpolation between the channels of the full energy peak. For each operating condition the spectroscopic data was typically averaged over three to five shots.

The variation of species composition as a function of accelerator current as measured by the optical and momentum analysis techniques is shown in Fig. 11. This is a composite of data for neutral beam energies of 120, 110, 100, 80, 60, and 40 keV with a gas flow of 17 Torr L/sec. At each energy measurements were made as the accelerator current was varied to provide a "tuning" curve for the determination of the minimum divergence angle and the corresponding optimum accelerator current. Thus there is some overlap between the data at different energies at least for $E \geq 100$ keV. In Fig. 12 we show the variation in the composition of the ion beam as the gas flow through the ion source and neutralizer is changed while the accelerating voltage is held fixed at 80 keV and the accelerator current is also constant. We find that the D^+ current remains constant within experimental uncertainties while D_2^+ is converted to D_3^+ as the gas pressure in the ion source increases. This is what one expects if the dominant process for producing D_3^+ in the source is $D_2^+ + D_2 \rightarrow D_3^+ + D$.[24]

A typical tuning curve for the variation of divergence angle perpendicular to the accelerator grids as a function of accelerator current is shown in Fig. 13. The points in the figure correspond to the 1/e half angle of the full energy component of the neutral beam obtained by this spectroscopic technique at an accelerator voltage of 110 keV. The curve is a parabola fitted to the experimental data. It is interesting that the experimental points fall close to the parabolic fit even for conditions well away from the minimum divergence. Similar results were obtained at the other accelerator voltages and from the least squares parabolic fit we can obtain the optimum accelerator current as a function of accelerator voltage. The results are shown in Fig. 14.

From the Child-Langmuir Law for space charge limited flow we expect the optimum accelerator current should scale with the 3/2 power of the accelerator voltage for an ion beam of a single species. The broken curve in the figure is for this $V^{3/2}$ scaling. For a mixed ion beam composed of species D^+, D_2^+, and D_3^+ the current density j, for space-charge limited flow in a plane-parallel diode, is reduced by a factor $F = j/j_0$ from the current density j_0 that would be obtained for a D^+ ion beam under the same conditions. Here $F = 1/(f_1 + \sqrt{2}f_2 + \sqrt{3}f_3)$ where f_1, and f_2, and f_3 are the fractional current densities of D^+, D_2^+, and D_3^+ ions. The solid curve in Fig. 14 is computed from F using the data of Fig. 11 for species ratios and normalized to pass through the 120 keV data point. The calculated curve is in good agreement with the experimental data points derived from the Doppler shift spectroscopy, showing that the perveance of the system is constant and that the observed deviation from the expected $V^{3/2}$ scaling is due to the changing beam composition.

Our analysis of divergence assumes that the gas density is constant along the optic axis. Since in this case the optic axis makes an angle of 60^0 to the neutral beam direction and the beam width perpendicular to the accelerator slots (x-direction) is 40 cm, the optical system is sampling one side of the beam 23 cm further downstream in the neutralizer than the location it samples on the other side of the beam. If we have a linear pressure drop along the neutralizer (molecular flow), then this implies a 10% variation in the gas density along the line of sight of the optics. Thus the Doppler shift spectroscopy will yield a weighted average of the local angular distribution function. This is the most extreme example of this effect on the neutral beamlines we have observed

since the optic axis is more nearly normal to the neutral beam axis and the width of the neutral beam is four times larger (x-direction) than in the case of the 10 by 10 cm sources. In the appendix we show that this effect is negligible in this case because we are observing in the "near field region", i.e. the angle subtended by the source from points along the optic axis, is large compared with the divergence of the neutral beam.

IV. Thick Target Approximation

A great simplification can be achieved in analyzing the spectroscopy data for species if one can assume a thick target. In the thick target approximation we assume that all molecular ions and molecules in the beam have dissociated and that each energy component in the beam has achieved the equilibrium ratio of protons to hydrogen atoms. The effective cross section for Doppler shifted Balmer alpha emission for an atomic hydrogen beam in a thick target is $\sigma_{EQ}(E) = F_+^\infty \sigma_+ + F_0^\infty \sigma_0$ where σ_+ and σ_0 are the optical excitation cross sections [9,10] for Balmer alpha emission by fast protons and hydrogen atoms respectively in hydrogen gas and F_+^∞ and F_0^∞ are the experimentally measured equilibrium fractions of fast protons and hydrogen atoms for a thick target.[16] The coefficient γ_i which we use in our species model is then proportional to $i \times \sigma_{EQ}(E_i)$ where $i = 1$, 2, and 3 for the full, half, and third energy components of the beam, because, for example, each H_2^+ produces two nucleons.

In Fig. 15 we plot $\sigma_{EQ}(E)$ as a function of the accelerating voltage for a hydrogen beam. The solid curve is $\sigma_{EQ}(E)$ computed from the measurements of F_+^∞, F_0^∞, σ_+, and σ_0 (including our extrapolation

of σ_0) in References (5), (6), and (12). The optical cross sections are unavailable below 10 keV for a hydrogen beam; however, in the series of measurements shown in Fig. 11 (where the target thickness is $\Pi = 1.6 \times 10^{16} cm^{-2}$) we have optical data as low as 40 keV for a deuterium beam -- this is dependent on optical cross sections at energies as low as 6.7 keV for an equivalent hydrogen beam. If we assume the species ratios correspond exactly to the solid curves in Fig. 11, then from the observed light intensity ratios we can calculate "experimental" γ coefficients including the 40 keV data for which we did not attempt the spectroscopic analysis of species. In Fig. 15 we plot measured values of $\sigma_{EQ}(E/i) = C\gamma_i/i$ for these non-thick target cases; C is adjusted so that $C\gamma_1$ falls along the theoretical curve. The experimental points fall reasonably close to the thick target calculation. It appears from this comparison that the thick target approximation can be used with good accuracy even in cases where the target is not thick, permitting great simplification in data analysis.

With this thick target approximation in Fig. 15 we can calculate the D_2O^+ relative current for a 120 keV deuterium beam produced by the 10 x 40 cm magnetic bucket source. We find that the D_2O^+ current density is approximately 0.8% of the total current density.

We have found that our computer model for analyzing species is not very sensitive to the assumed target thickness and therefore there is not a large difference between results obtained using it and those obtained using the thick target approximation. For a 120 keV deuterium neutral beam (of species ratio $D^+:D_2^+:D_3^+ = 75 : 15 : 10$) the two models differ by less than 1% in their estimate of D^+ fraction for

target thicknesses $\Pi > 5 \times 10^{15} cm^{-2}$ if the cross section for $\underline{D}_2 + D_2 \rightarrow \underline{D}^*$ is neglected For comparison, if the latter cross section is arbitrarily set equal to the corresponding cross section for D_2^+ then the two models still differ by less than 3% for $\Pi > 5 \times 10^{15} cm^{-2}$. The spectroscopic species analysis is somewhat more sensitive to target thickness for a 120 keV hydrogen neutral beam. For a hydrogen neutral beam of the same species ratio, the thick target approximation differs from the computer model by less than 5% in the estimated H^+ fraction for $\Pi > 10^{16} cm^{-2}$. If we set $\sigma(H_2) = \sigma(H_2^+)$ the models differ by less than 6% for $\Pi > 10^{16}\ cm^{-2}$.

From the agreement we have observed between this spectroscopic measurement of species and momentum analysis we conclude that the spectral analysis based on the cross sections we have used has an accuracy comparable to the momentum analysis. We believe the spectroscopic analysis of species can be further improved by an accurate measurement of the effective cross section $\sigma_{EQ}(E)$ (particularly the relative cross section as a function of energy) for Balmer alpha emission from a hydrogen beam in a thick target. The individual optical cross sections and the charge exchange cross sections important in the neutralizer are then required only to make a relatively small correction for finite target thickness to a baseline provided by $\sigma_{EQ}(E)$.

Appendix

I. Coupling between θ_x and θ_y measurements

Because the Doppler shift is determined only by the angle between the optic axis and a neutral atom trajectory, there is a slight coupling between the divergence measurements in the two different directions. If the z-axis is along the centerline of the neutral beam axis and the x and y axes are perpendicular and parallel to the grids of the ion source, then the direction of a unit vector, $\hat{v}$, parallel to the velocity of a particle in the neutral beam can be expressed in terms of the angles θ_x and θ_y that $\hat{v}$ makes with the y-z plane and the x-z plane respectively. The direction cosines of $\hat{v}$ in the x and y directions are then $\sin\theta_x$ and $\sin\theta_y$ respectively. If the optic axis is in the y-z plane making an angle θ_{oy} with the neutral beam axis, then the angle θ between the particle trajectory $\hat{v}$ and the optic axis is:

$$\theta = \cos^{-1}\left\{\cos(\theta_{oy} - \theta_y) + \cos\theta_{oy}\cos\theta_x\left(\sqrt{1 - \frac{\sin^2\theta_x}{\cos^2\theta_y}} - 1\right)\right\} \quad (5)$$

If $\theta_x \ll \theta_{oy}$ the second term in the brackets is small compared to the first term and we can expand in powers of $\sin\theta_x$ and we find:

$$\theta = \theta_{oy} - \theta_y + 1/2\,\frac{\cos\theta_{oy}}{\cos\theta_y}\,\frac{\sin^2\theta_x}{\sin(\theta_{oy}-\theta_y)} \quad (6)$$

Note that the third term is quadratic in the small quantity $\sin\theta_x$. If θ_y is also a small angle, as in our case, the correction term is

approximately $1/2 \sin^2 \theta_x / \tan \theta_{oy}$. For a typical case in our experiment $\theta_{oy} = 78^\circ$, $\theta_y = 0.0^0$, and $\theta_x = 1.5^\circ$, the third term in (6) is 0.004° as illustrated in Fig. 1. Thus the coupling between the divergence measurements in the two directions is very small and we have neglected it in our analysis.

II. Effect of optical acceptance angle

The importance of the acceptance angle of the optical system to the measurement of divergence can be determined if we calculate the broadening of a bi-Gaussian beam viewed with a finite optical acceptance angle. The distribution in wavelength of the spectral line can be expressed in terms of error functions:

$$F_\lambda = \frac{C}{\sin \theta(\lambda)} \operatorname{erf}[(\theta(\lambda) - \theta_{ox} + \alpha)/\theta_{ex}] - \operatorname{erf}[(\theta(\lambda) - \theta_{ox} - \alpha)/\theta_{ex}] \tag{7}$$

where θ_{ox} is the angle between the optic axis and the z axis, $\theta(\lambda)$ is the angle obtained by solving equation (1), for θ_{ex} is the divergence in the x-z plane of the bi-Gaussian neutral beam, C is a constant, and α is the half-angle of the light rays accepted by the optical system. The difference between the error functions approaches a Gaussian and deviates from a Gaussian by a lowest order term which is quadratic in α as α goes to zero. $F(\lambda)$ is not exactly a Gaussian since $\theta(\lambda)$ is not a linear function of λ; from (1) we have:

$$\theta_x(\lambda) = \theta(\lambda) - \theta_{ox} = \cos^{-1}\left\{(1 - \sqrt{1-\beta^2}\ \lambda/\lambda_o)/\beta\right\} - \theta_{ox} \qquad (8)$$

Let $\Delta\lambda = \lambda - \lambda_1$ where $\theta(\lambda) = \theta_{ox}$ where λ_1 is the central wavelength of a Doppler shifted and broadened line. Rearranging equation (8) we have:

$$\theta_x(\Delta\lambda) = \cos^{-1}\left\{\frac{1}{\beta}\left(1 - \frac{\lambda_1}{\lambda_o}\sqrt{1-\beta^2}\right) + \frac{1}{\beta}\frac{\Delta\lambda}{\lambda_o}\sqrt{1-\beta^2}\right\} - \theta_o \qquad (9)$$

Since the second term in the brackets is small compared to the first we make a Taylor expansion of the arc cosine about the first term and we find:

$$\theta_x(\Delta\lambda) = -\frac{\frac{\Delta\lambda}{\lambda_o\beta}\sqrt{1-\beta^2}}{\sin\theta_o}\left\{1 + \frac{\frac{\Delta\lambda}{\lambda_o\beta}\sqrt{1-\beta^2}}{2\tan\theta_o \sin\theta_o} + \cdots\right\} \qquad (10)$$

The second term in the expansion is small and can be neglected provided the angle between the optic axis and the neutral beam is not too shallow. In our system the second term above is less than 0.01 if $\theta_x < 2^\circ$. The slight assymetry caused by the sin $\theta(\lambda)$ factor in $F(\lambda)$ is also negligible under these conditions. For range of collection angles α we have calculated the 1/e halfwidth $\Delta\lambda_e$ of the distribution $F(\lambda)$ according to (7). We find that the "observed" divergence angle, $(\theta_{ex})_{obs}$, is slightly larger than the true divergence θ_{ex} of the Gaussian beam according to the relation: $(\theta_{ex})^2_{obs} = \theta^2_{ex} + (c\alpha)^2$ where $(\theta_{ex})_{obs} = \frac{\Delta\lambda_e\sqrt{1-\beta^2}}{\lambda_o\beta\sin\theta_o}$ and $c = .85 \pm .1$ for $\alpha < 0.5^\circ$ and $0.4 < \theta_{ex} < 1.6^\circ$. Since the dependence on α is quadratic the correction can be made quite small and is less than 0.03° in our system.

III. Emittance

To calculate the importance of the variation of gas density with position in the neutralizer on the measurement of divergence we consider the emittance function $\varepsilon(x,y,z,\theta_x,\theta_y)$ which we define as the equivalent current per unit area per unit solid angle at the location x,y,z (where the z axis is along the centerline of the neutral beam) and in the direction defined by θ_x and θ_y. For a source function which is assumed to be bi-Gaussian we have at the source:

$$\varepsilon(x,y,o,\theta_x,\theta_y) = \frac{4j(x,y)}{\pi\theta_{ex}\theta_{ey}} \; e^{-(\theta_x/\theta_{ex})^2} \; e^{-(\theta_y/\theta_{ey})^2} \qquad (11)$$

where $j(x,y)$ is the source current density which is assumed to be uniform over the accelerator area and of course zero everywhere else in the $z = 0$ plane, θ_{ex} and θ_{ey} are the 1/e half angle divergences perpendicular to and parallel to the accelerator slots. Then at a location x,y,z downstream in the neutralizer we have (assuming particles follow straight line trajectories after leaving the accelerator):

$$\varepsilon(x,y,z,\theta_x,\theta_y) = \frac{4j(x',y')}{\theta_{ex}\theta_{ey}} \; e^{-(\theta_x/\theta_{ex})^2} \; e^{-(\theta_y/\theta_{ey})^2} \qquad (12)$$

where $x = x - \theta_x z$ and $y = y - \theta_y z$. The emittance downstream in the direction θ_x,θ_y is the same as the corresponding emittance in the

source plane at the location x , y , 0 which is the interaction of the particle trajectory with the source plane.

Since the spectral analysis for an optic axis in the x-z plane is insensitive to the angle θ_y a trajectory makes with the x-z plane we need only consider the emmitance defined in the x-z plane:

$$\epsilon_x(x,z,\theta_x) = \frac{2j_x(x')}{\sqrt{\pi}\,\theta_{ex}} e^{-(\theta_x/\theta_{ex})^2} \tag{13}$$

where $x' = x - \theta_x z$ and $j_x(x')$ is the line density of current at the source ($j_x(x) = \int_{-\infty}^{\infty} j(x,y)dy$). Then the spectral analysis will measure an angular distribution $F(\theta_x)$:

$$F(\theta_x) = \int_{-s_1}^{s_1} \epsilon_x(x(s),z(s),\theta_x)\rho(z(s))ds \tag{14}$$

This is a line integral over the optic axis within the limits of the neutralizer box, where s is the distance along the optic axis, $x(x) = s \sin\theta_{ox}$, $z(s) = z_0 + s\cos\theta_{ox}$, $\rho(z)$ is the gas density at a distance z from the source, θ_{ox} is the angle of the optic axis with the z axis, and z_0 is the distance from the source to the optic axis along the centerline of the neutral beam. We find by a numerical solution to this integral for a 40 cm wide source and $\theta_{ex} = 1.00^o$ that the **change in line width caused by a 10% linear variation in gas density along the optical path is less than 1% of the full line width.**

The reason the spectroscopic analysis is not very sensitive to variation in gas density is that we are in the "near field" region of the neutral beam. The angle subtended by the source at the intersection of

($\theta_{source} << \theta_{ex}$) the direction of particle trajectories are strongly correlated with the location in the x-y plane. Therefore, for the measurement of divergence by the Doppler broadening of Balmer emission it is desirable to observe the neutral beam in the near field region, that is, near the source.

We would like to acknowledge the help of Dexter Massoletti, Loren Shalz, Klaus Berkner, other members of the LBL MFE group, and also helpful discussions with T. Orzechowski of LLL, and J. F. Bonnal of Association Euratom-CEA Sur La Fusion and helpful discussions with the representatives of the equipment manufacturers used in this experiment.

References

1. W. R. Baker, K. H. Berkner, W. S. Cooper, K. W. Ehlers, W. B. Kunkel, R. V. Pyle, and J. W. Stearns, LBL-3208 (1974).
2. K. W. Ehlers, K. H. Berkner, W. S. Cooper, J. M. Haughian, W. B. Kunkel, B. A. Prichard, Jr., R. V. Pyle, and J. W. Stearns, LBL-4471 (1976).
3. C. F. Burrell, W. S. Cooper, W. F. Steele and R. R. Smith in: Proc. 7th Symp. on Engineering Problems of Fusion Research (Knoxville 1977) IEEE (1977) 374.
4. K. H. Berkner, C. F. Burrell, C.-F. Chan, W. S. Cooper, R. R. Smith, W. F. Steele, and J. W. Stearns, Bull. Amer. Phys. Soc. 23, 913 (1978).
5. M. Ulrickson and J. P. Bussac in: Intern. Conf. on Plasma Science (Monterey, CA) IEEE (1978) 18.
6. J. F. Bonnal, G. Bracco, C. Breton, C. De Michelis, J. Druaux, M. Mattioli, R. Oberson and J. Ramette, Phys. Lett. 75A, 65 (1979).
7. Philip R. Bevington, Data Reduction and Error Analysis for the Physical Sciences, McGraw-Hill, New York 1969.
8. Frank R. Pomilla, Astrophys. J. 148, 559 (1967).
9. R. H. Hughes, H. M. Petefish, and H. Kisner, Phys. Rev. A5, 2103 (1972).
10. R. H. Hughes, Sabrina Lin, and L. L. Hatfield, Phys. Rev. 130, 2318 (1963).
11. L. L. Hatfield and R. H. Hughes, Phys. Rev. 131, 2556 (1963).
12. L. C. Johnson, Astrophys. J. 174, 227 (1972).

13. D. H. Sampson and L. B. Golden, Astrophys. J. 186, 695 (1973).

14. I. C. Percival, Nucl. Fusion 6, 182 (1966).

15. J. G. Lodge, I. C. Percival, and D. Richards, J. Phys. B9, 239 (1976).

16. S. K. Allison and M. Garcia-Munoz in Atomic and Molecular Processes, D. R. Bates, ed., Academic Press, New York (1962).

17. A. Guthrie and R. K. Wakerling, Vacuum Equipment and Techniques, McGraw-Hill Co., New York (1949).

18. K. H. Berkner, R. V. Pyle, and J. W. Stearns, Nuclear Fusion 15, 249 (1975).

19. K. F. Schoenberg, Rev. Sci. Instrum. 49, 1377 (1978).

20. D. A. Dunn and S. A. Self, J. Appl. Phys. 35, 113 (1964).

21. C. F. Burrell, W. S. Cooper, W. F. Steele, and R. R. Smith, LBL-6383 (1977).

22. A. B. Wittkower, P. H. Rose, P. P. Bastide, and N. B. Brooks, Phys. Rev. 136, A1254 (1964).

23. K. W. Ehlers and K. N. Leung, Rev. Sci. Instrum. 50, 1353 (1979).

24. C. F. Giese and W. B. Maier, II, J. Chem. Phys. 39, 739 (1963).

Figure Captions

Fig. 1 Coupling between the two directions of observation.

Fig. 2 Wavelength calibration near H_β with the lines of neon.

Fig. 3 Schematic diagram of data analysis.

Fig. 4 Cross sections for the production of Balmer alpha and beta radiation in the collision $\underline{H}^0 + H_2 \rightarrow \underline{H}^*$.

Fig. 5 Typical O.M.A. data spectrum. Red shifted lines from the 95 keV deuterium beam, viewed along an optic axis perpendicular to the accelerator slots, are to the right of the large unshifted D_α lines; to the left are the blue shifted lines from the beam viewed along an optic axis parallel to the accelerator slots.

Fig. 6 Computer generated reduced data display for a 95 keV deuterium neutral beam. In the upper half are the results for observation parallel to the accelerator slots; the lower half corresponds to observation perpendicular to the accelerator slots.

Fig. 7 Tuning curve: Sweep of beam current to find minimum divergence angle. Open hexagons are calorimetric data; filled symbols are spectroscopic data: circles -- full energy, triangles -- half energy, and squares -- third energy.

Fig. 8 Divergence angle parallel to the accelerator slots, for a 115 keV hydrogen beam, as a function of distance into the neutralizer.

Fig. 9 Comparison of species measurements by mass spectrometry and by Doppler shift spectroscopy.

Fig. 10 Time resolved spectroscopic measurement of species and relative D_2O^+ impurity concentration.

Fig. 11 Ion species composition as a function of accelerator current as the gas flow is held fixed.

Fig. 12 Ion species composition for an 80 keV deuterium beam as a function of the gas flow through the ion source.

Fig. 13 Divergence perpendicular to the accelerator slots of the full energy component of a 110 keV deuterium beam as a function of accelerator current.

Fig. 14 Scaling of optimum beam current (for minimum divergence) as a function of the beam voltage.

Fig. 15 Effective cross section for the emission of Balmer alpha radiation by fast hydrogen atoms in a thick target as a function of beam energy (solid curve), and experimentally measured data points (normalized) for a non-thick target (solid dots).

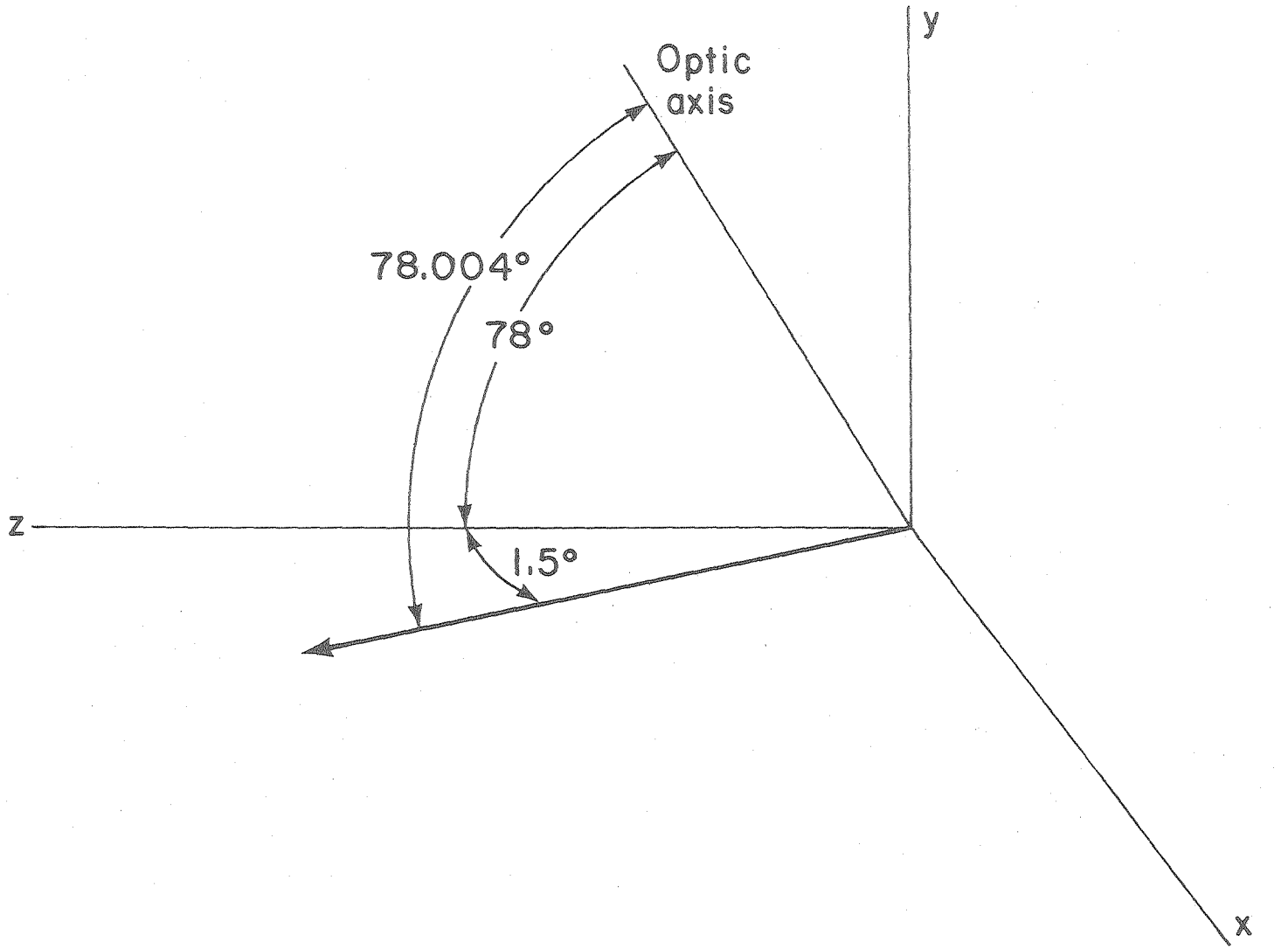

XBL 794-1245A

Fig. 1

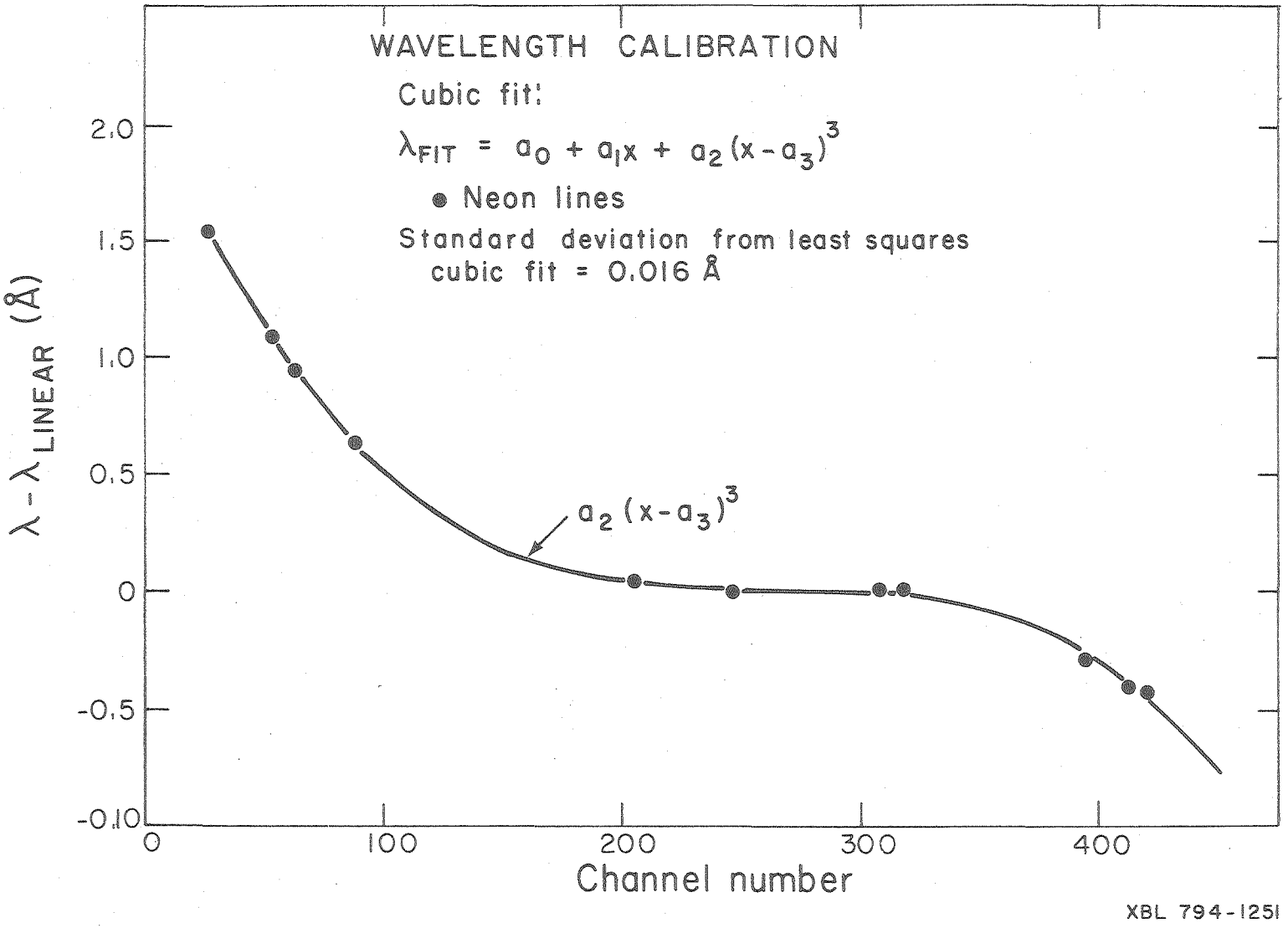
WAVELENGTH CALIBRATION
Cubic fit:
$\lambda_{FIT} = a_0 + a_1 x + a_2 (x - a_3)^3$
Neon lines
Standard deviation from least squares cubic fit = 0.016 Å
$a_2 (x - a_3)^3$
$\lambda - \lambda_{LINEAR}$ (Å)
2.0
1.5
1.0
0.5
0
-0.5
-0.10
0
100
200
300
400
Channel number
XBL 794-1251

Fig. 2

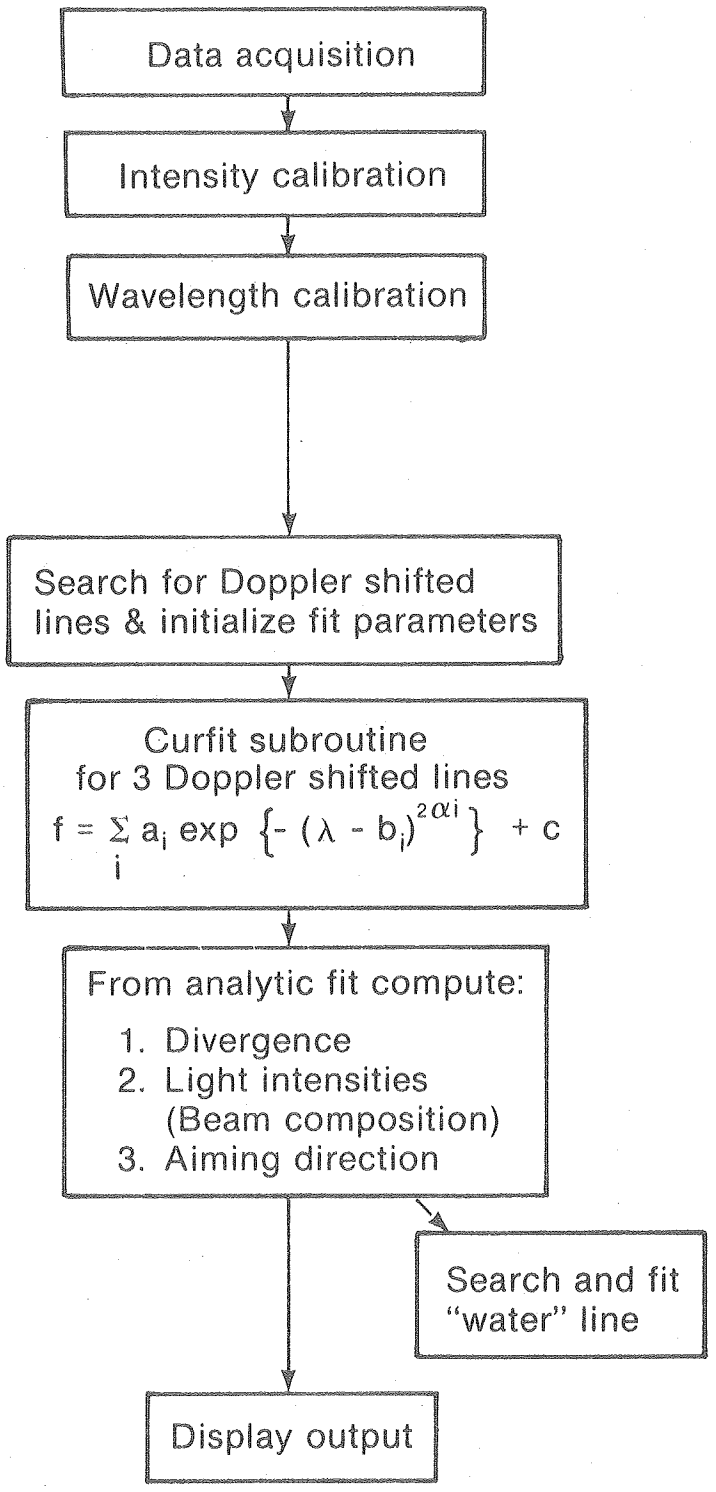
Data acquisition
Intensity calibration
Wavelength calibration
Search for Doppler shifted lines & initialize fit parameters
Curfit subroutine for 3 Doppler shifted lines
$f = \sum_i a_i \exp \{- (\lambda - b_i)^{2\alpha i}\} + c$
From analytic fit compute:
1. Divergence
2. Light intensities (Beam composition)
3. Aiming direction
Search and fit "water" line
Display output
XBL 794-1252

Fig. 3

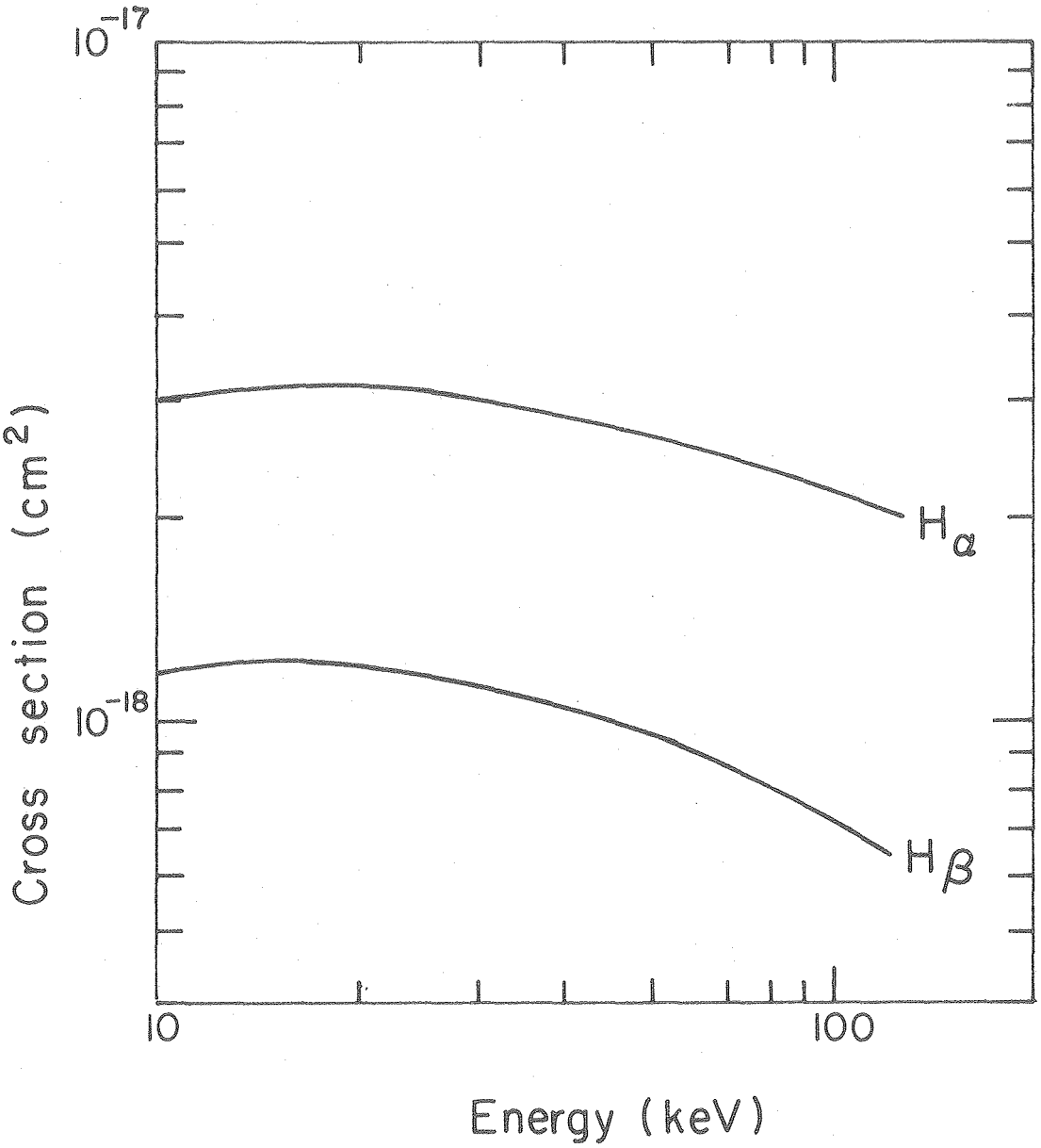

XBL7912-13382

Fig. 4

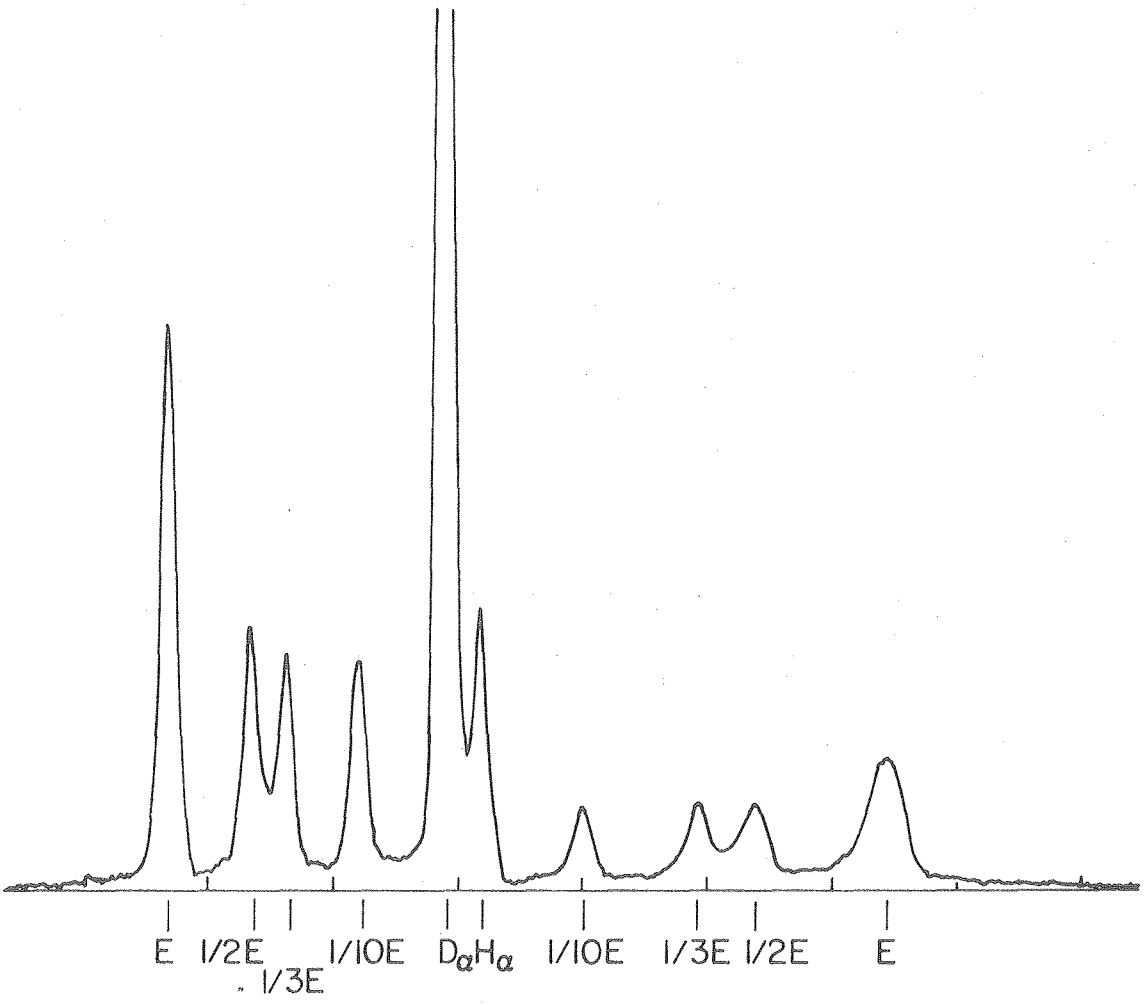

XBL 7912 - 13384

Fig. 5

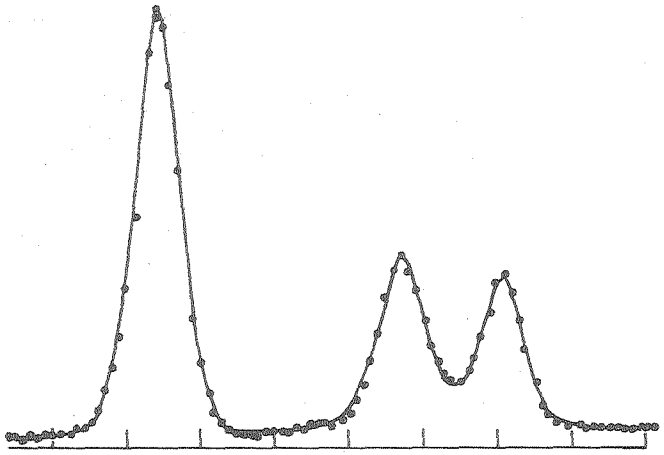

E	Light / Comp. (%)		Angle (deg.)		Divergence (deg.)	
1	55.0	80	-0.49	(0.01)	0.40	(0.02)
2	25.2	13	-0.48	(0.01)	0.65	(0.05)
3	19.8	7	-0.67	(0.02)	0.71	(0.06)

Theta = 78

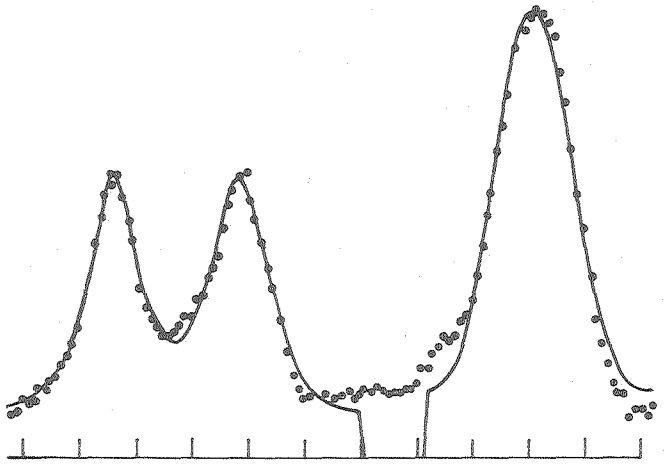

E	Light / Comp. (%)		Angle (deg)		Divergence (deg.)	
1	49.9	76	-0.56	(0.03)	1.09	(0.06)
2	25.7	15	-0.53	(0.07)	1.27	(0.14)
3	24.4	9	-0.41	(0.08)	1.33	(0.21)

Theta = 110.99

XBL 7912-13383

Fig. 6

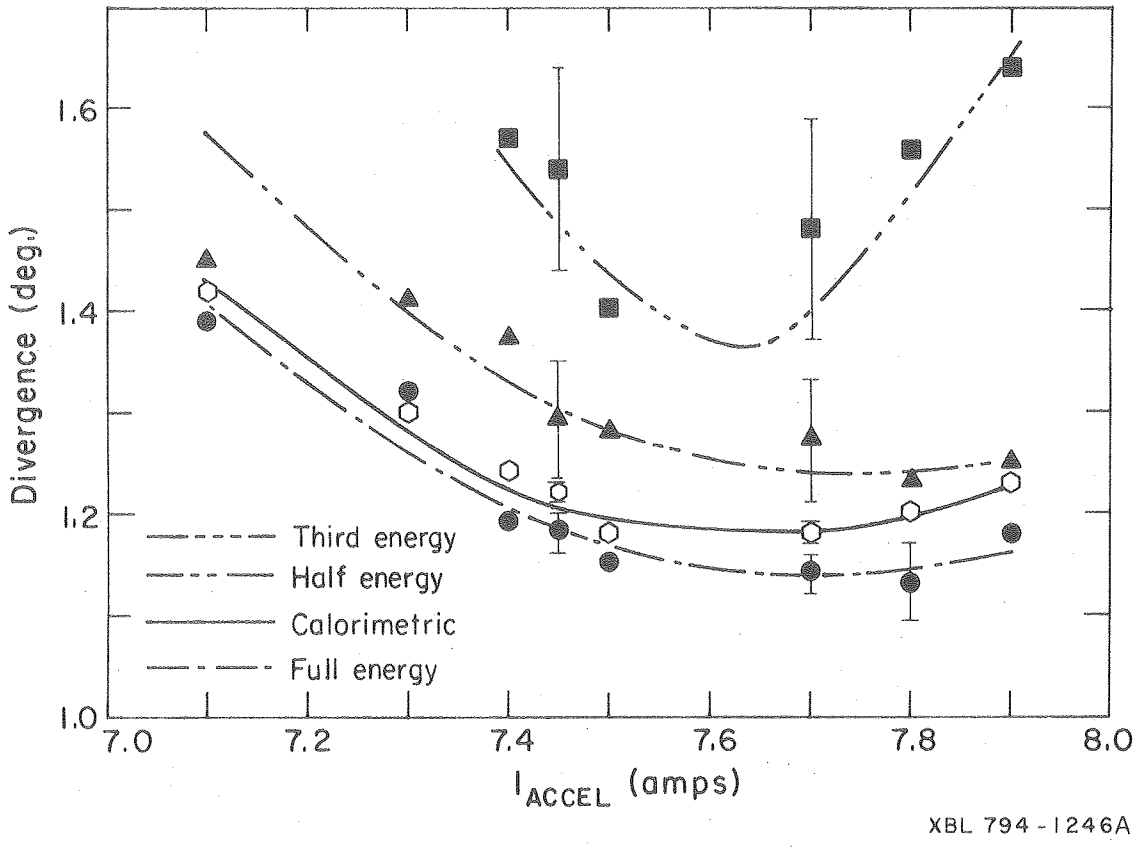
Divergence (deg.)
1.6
1.4
1.2
1.0
7.0
7.2
7.4
7.6
7.8
8.0
I ACCEL (amps)
Third energy
Half energy
Calorimetric
Full energy
XBL 794-1246A

Fig. 7

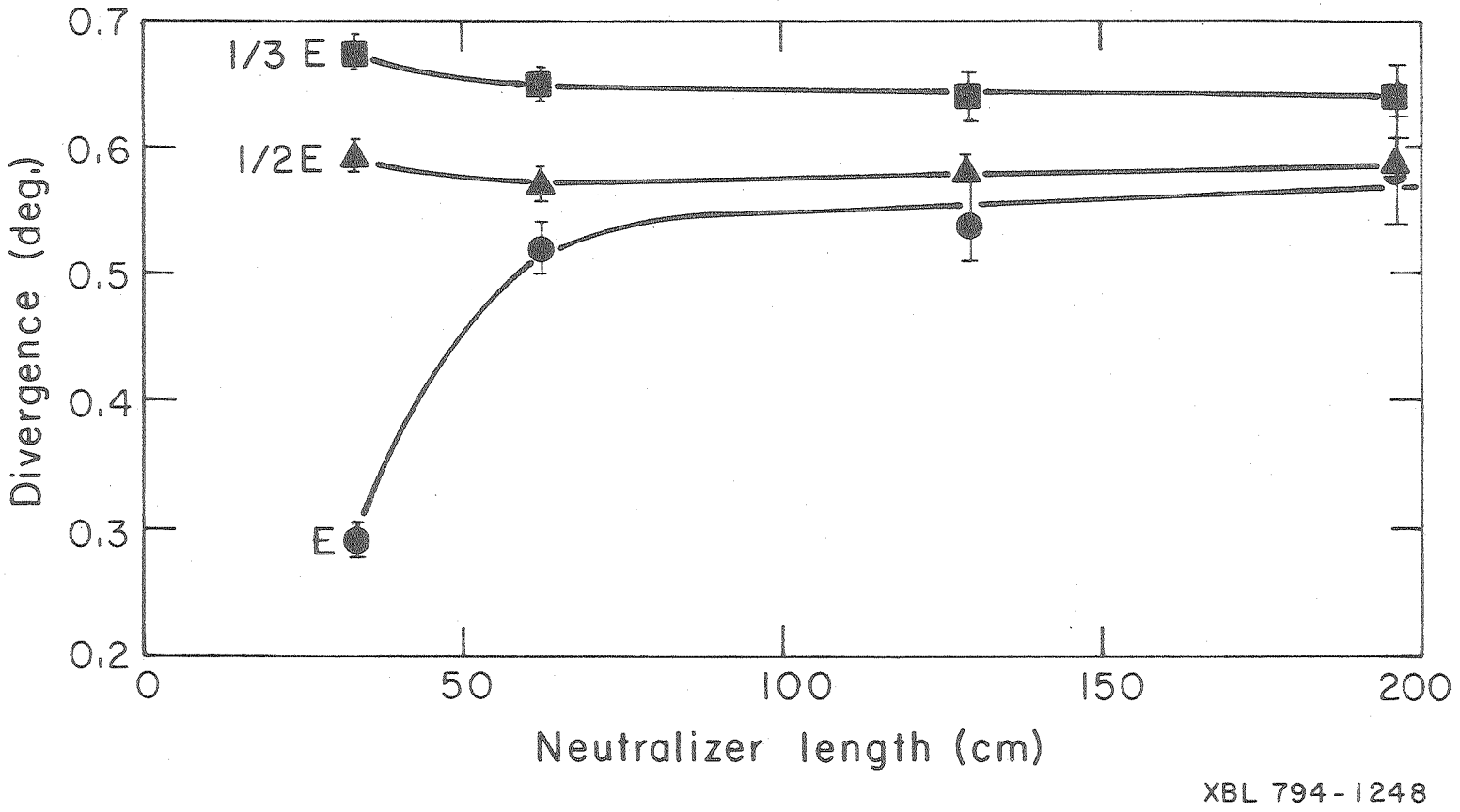
0.7
0.6
0.5
0.4
0.3
0.2
Divergence (deg.)
1/3 E
1/2E
E
0
50
100
150
200
Neutralizer length (cm)
XBL 794-1248

Fig. 8

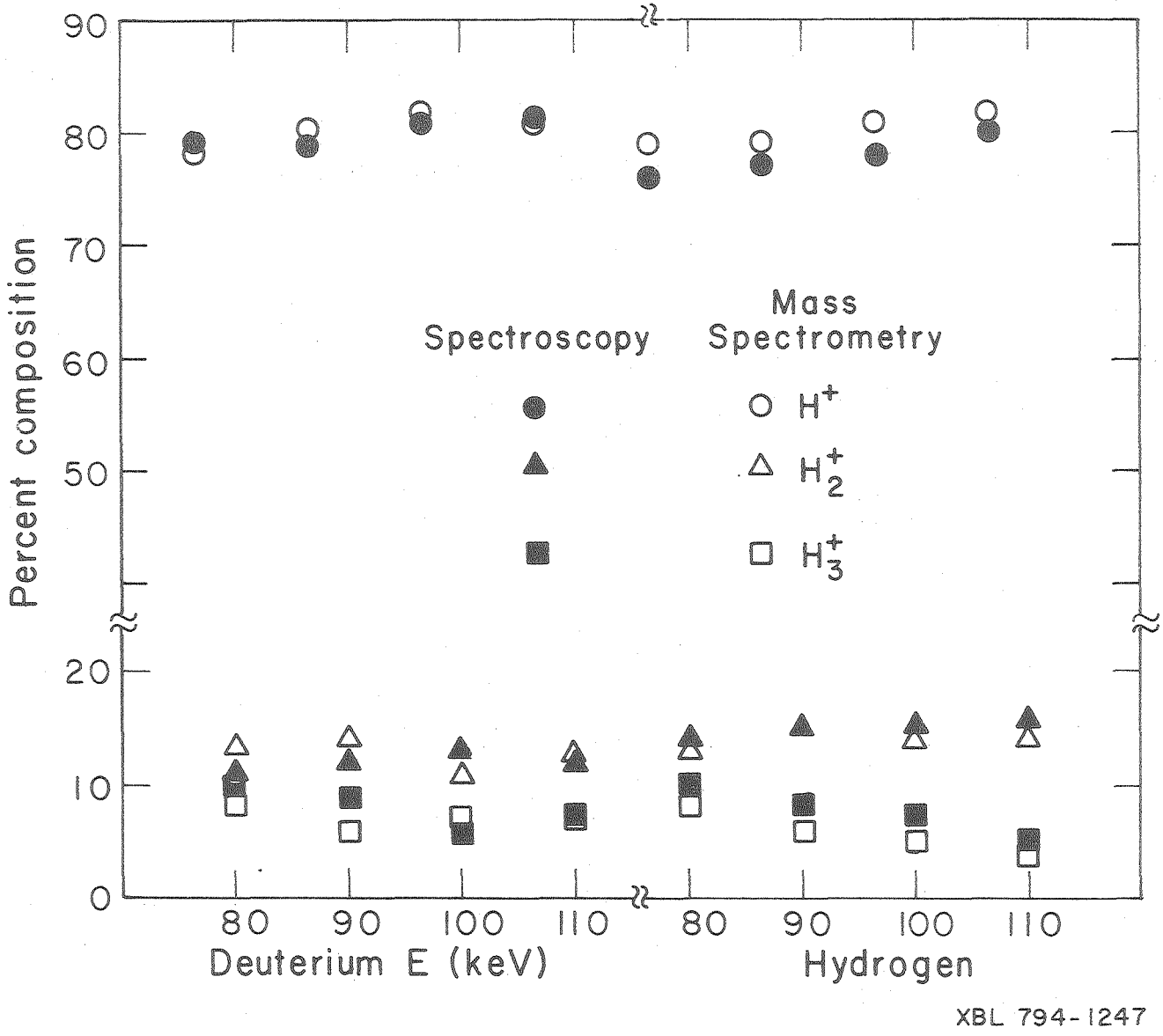
90
80
70
60
50
20
10
0
Percent composition
Spectroscopy
Mass Spectrometry
H+
H2+
H3+
80
90
100
110
Deuterium E (keV)
80
90
100
110
Hydrogen
XBL 794-1247

Fig. 9

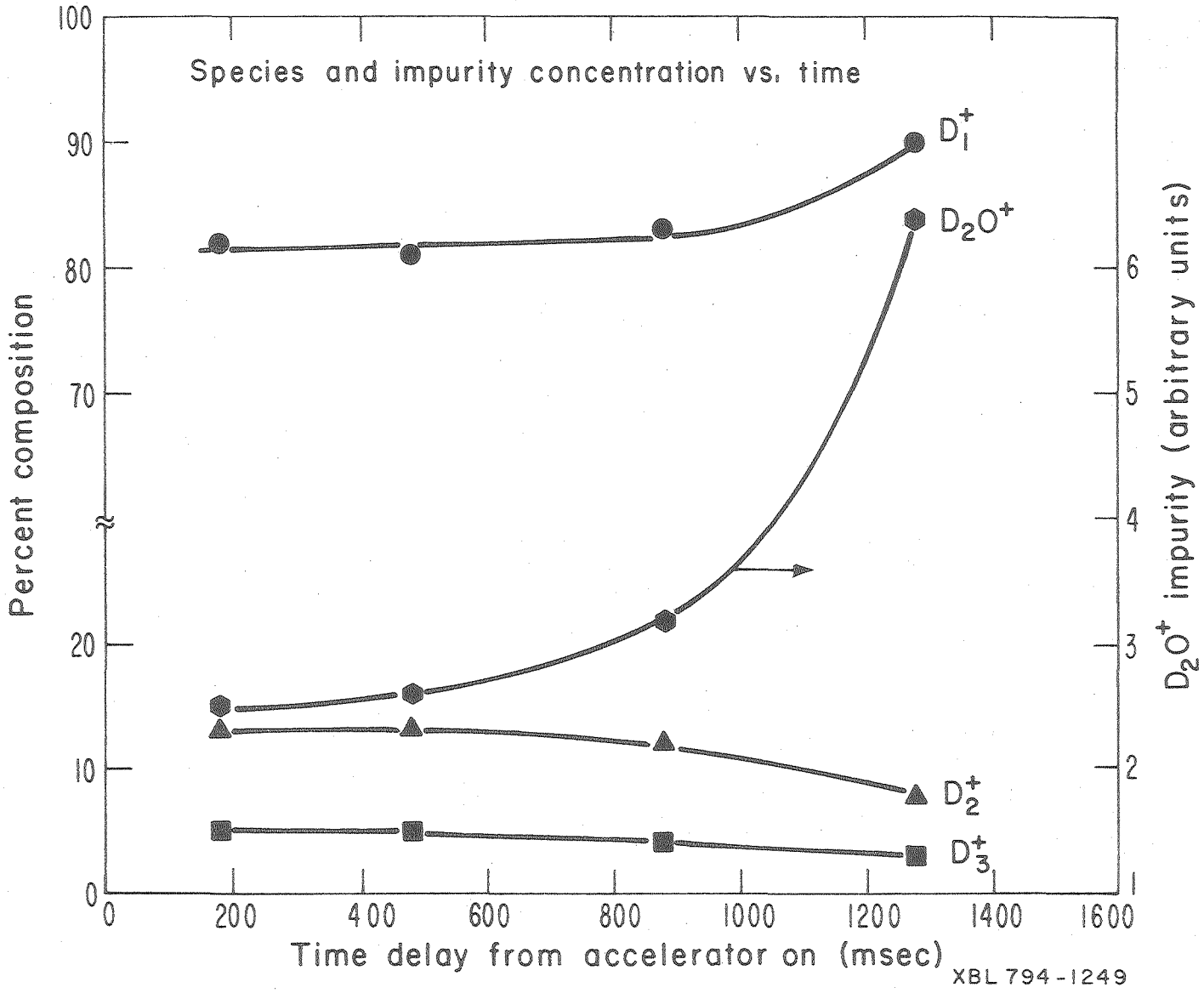
Species and impurity concentration vs. time
Percent composition
D_2O^+ impurity (arbitrary units)
Time delay from accelerator on (msec)
D_1^+
D_2O^+
D_2^+
D_3^+
100
90
80
70
20
10
0
6
5
4
3
2
1
0
200
400
600
800
1000
1200
1400
1600
XBL 794-1249

Fig. 10

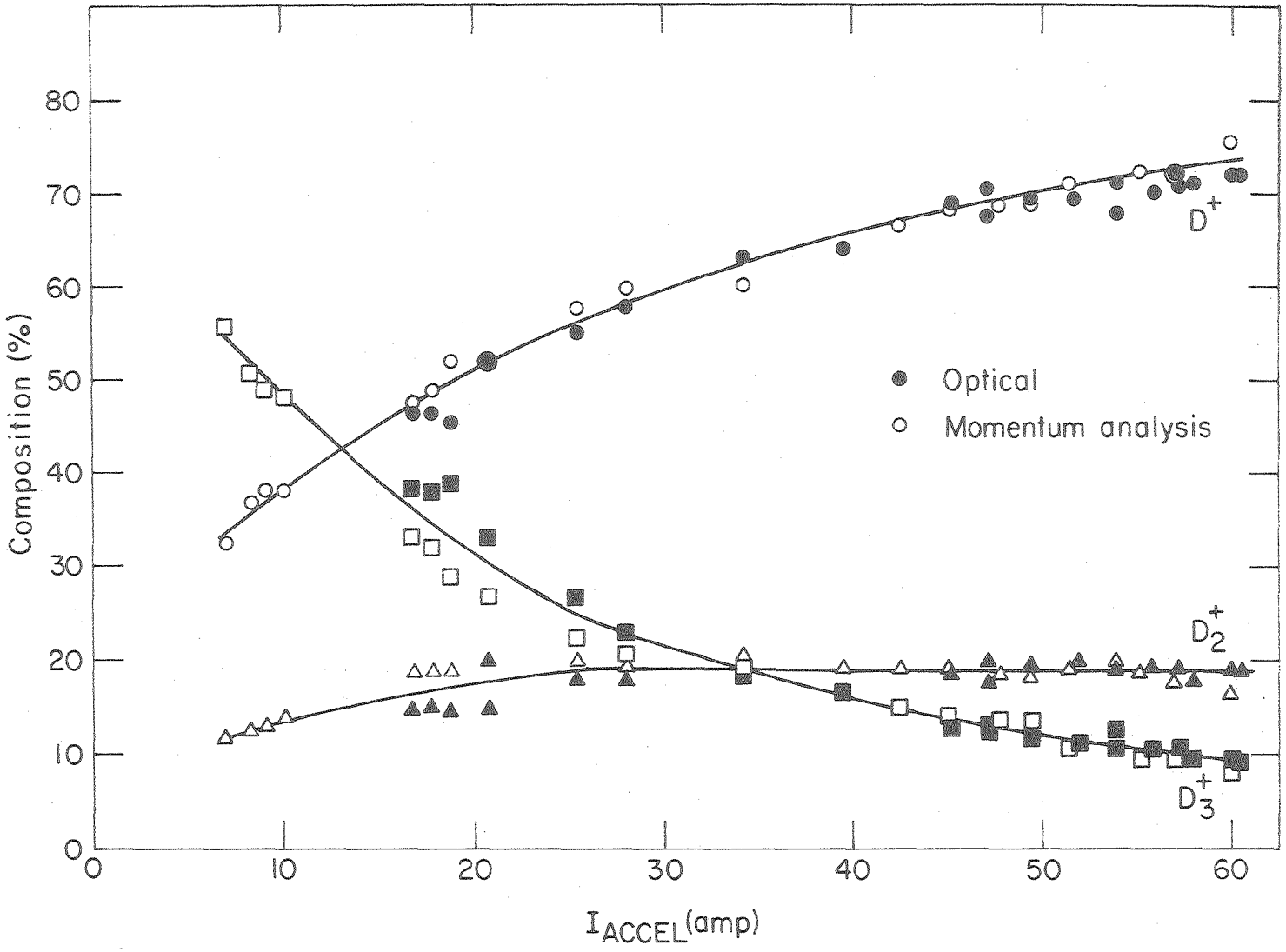
Composition (%)
80
70
60
50
40
30
20
10
0
0
10
20
30
40
50
60
I_{ACCEL}(amp)
Optical
Momentum analysis
D^+
D_2^+
D_3^+
XBL 7912-13386

Fig. 11

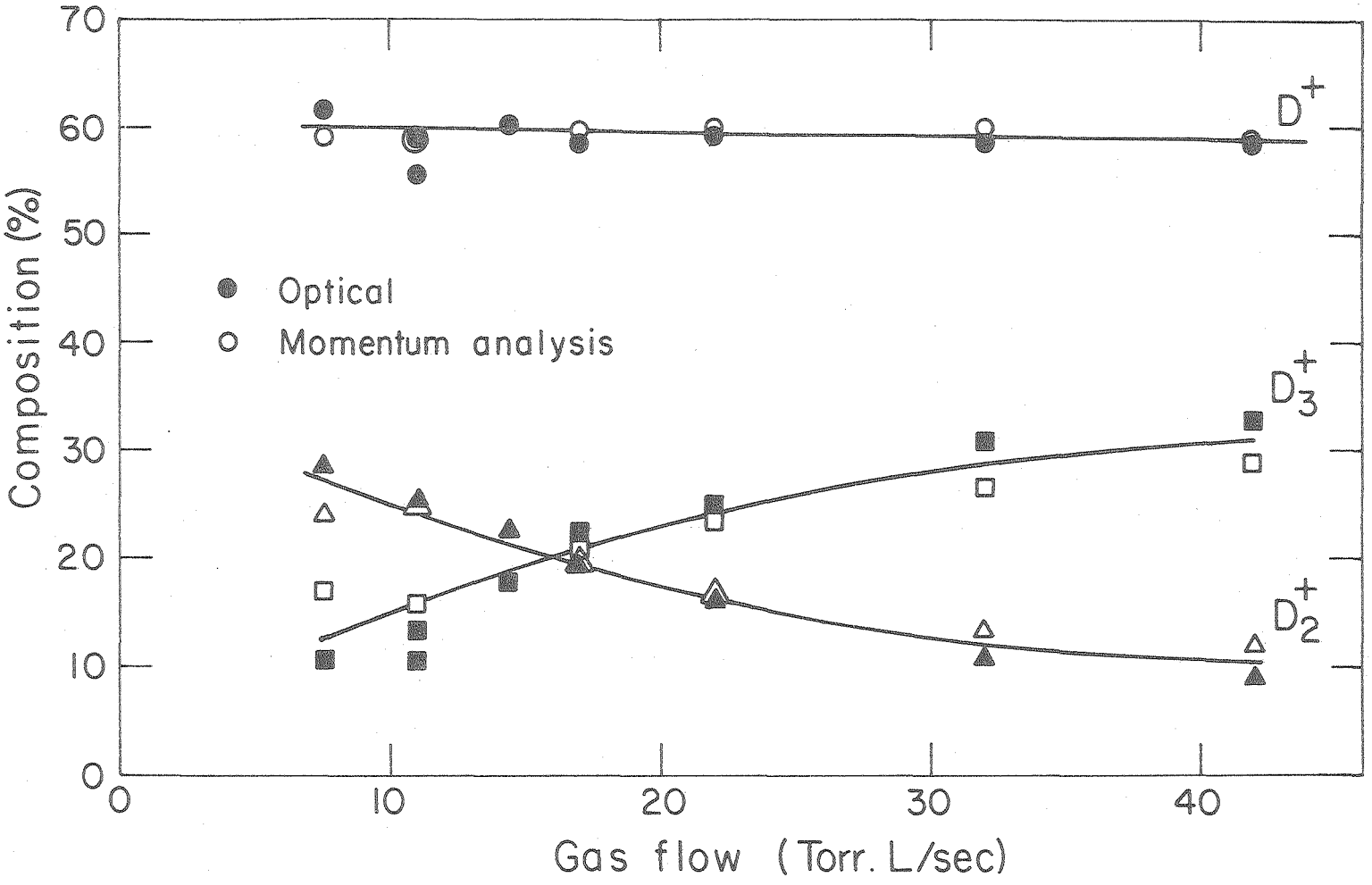

XBL 7912-13385

Fig. 12

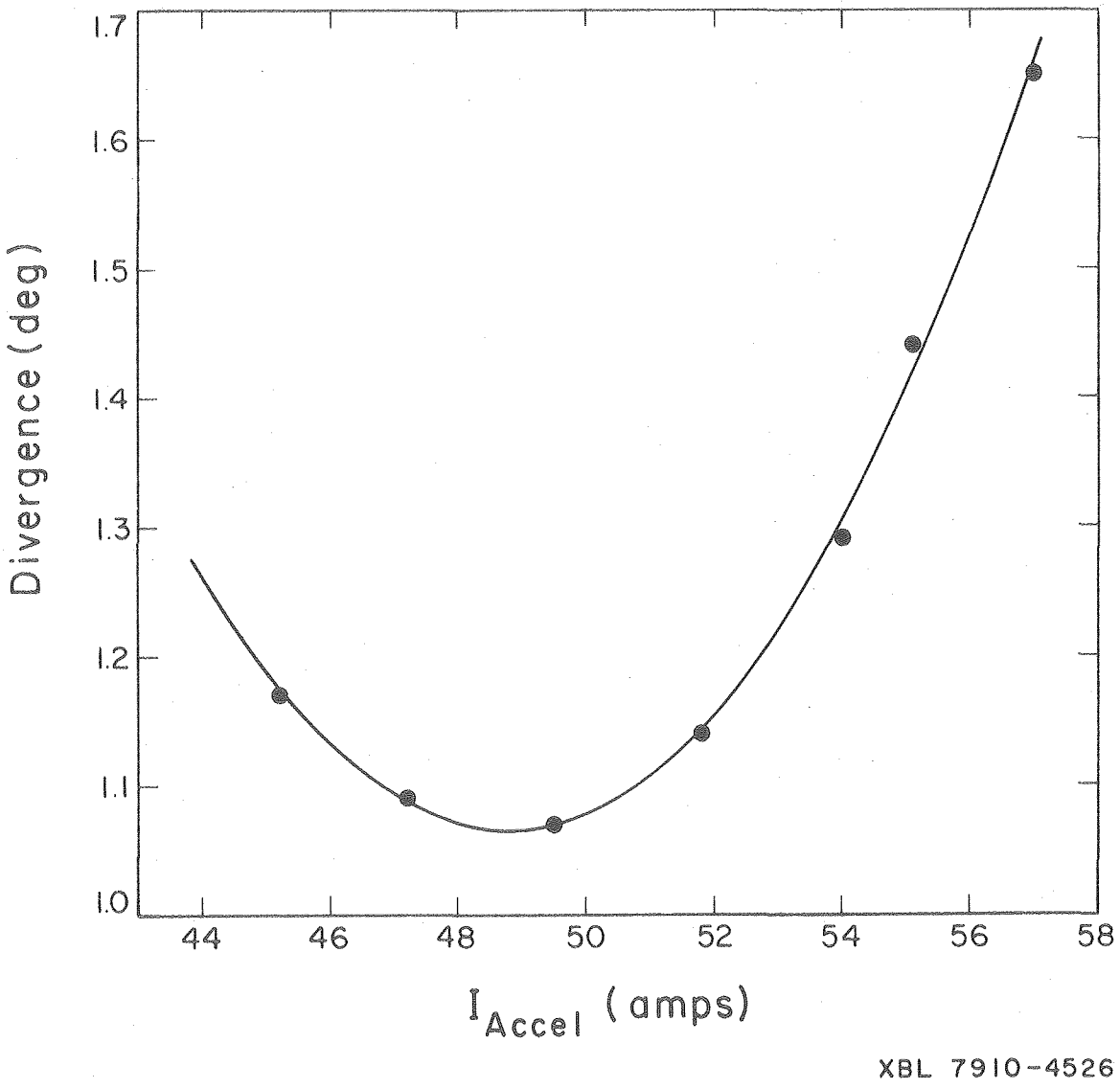
Divergence (deg)
1.7
1.6
1.5
1.4
1.3
1.2
1.1
1.0
44
46
48
50
52
54
56
58
I Accel (amps)
XBL 7910-4526

Fig. 13

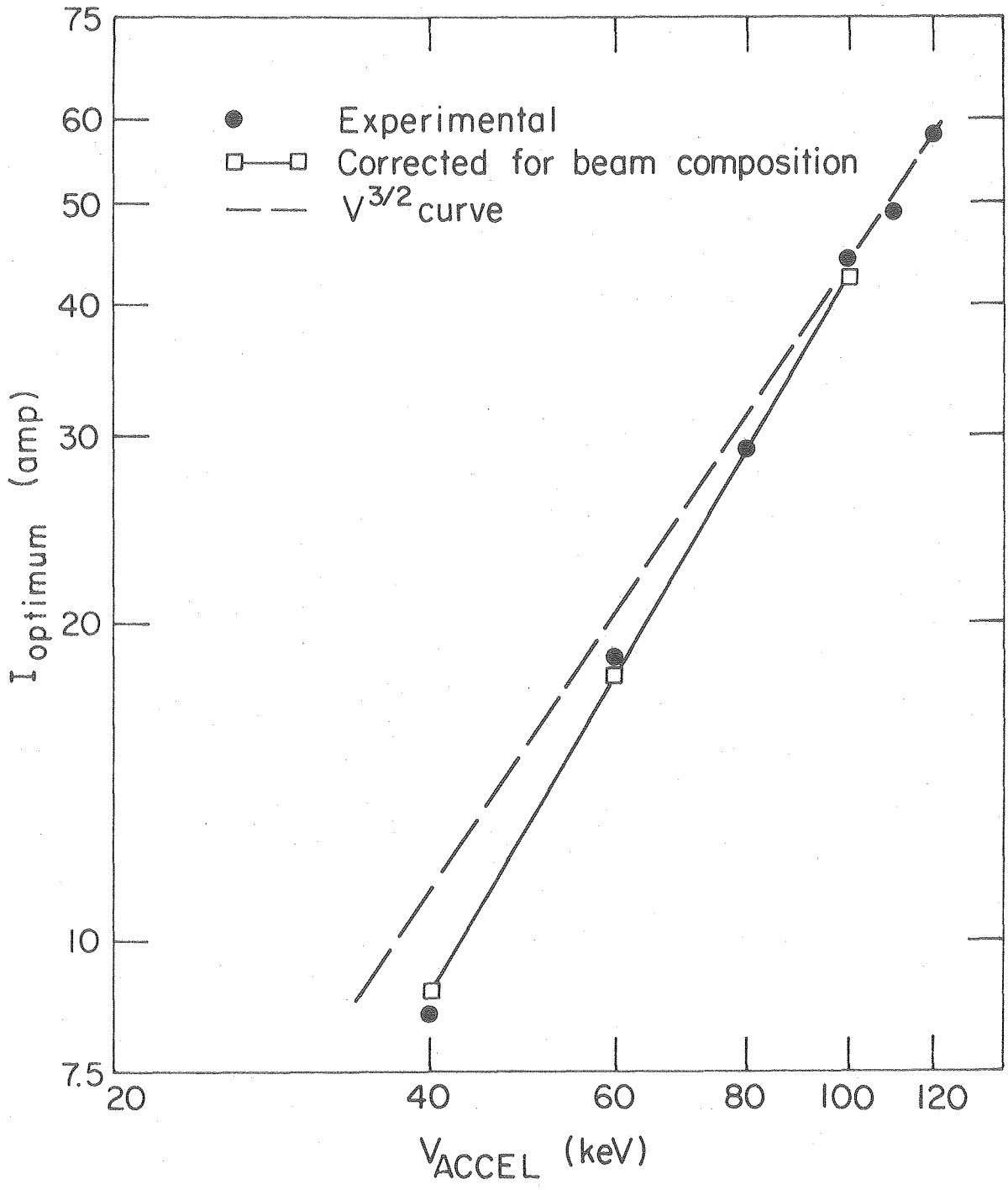

XBL7912-13387

Fig. 14

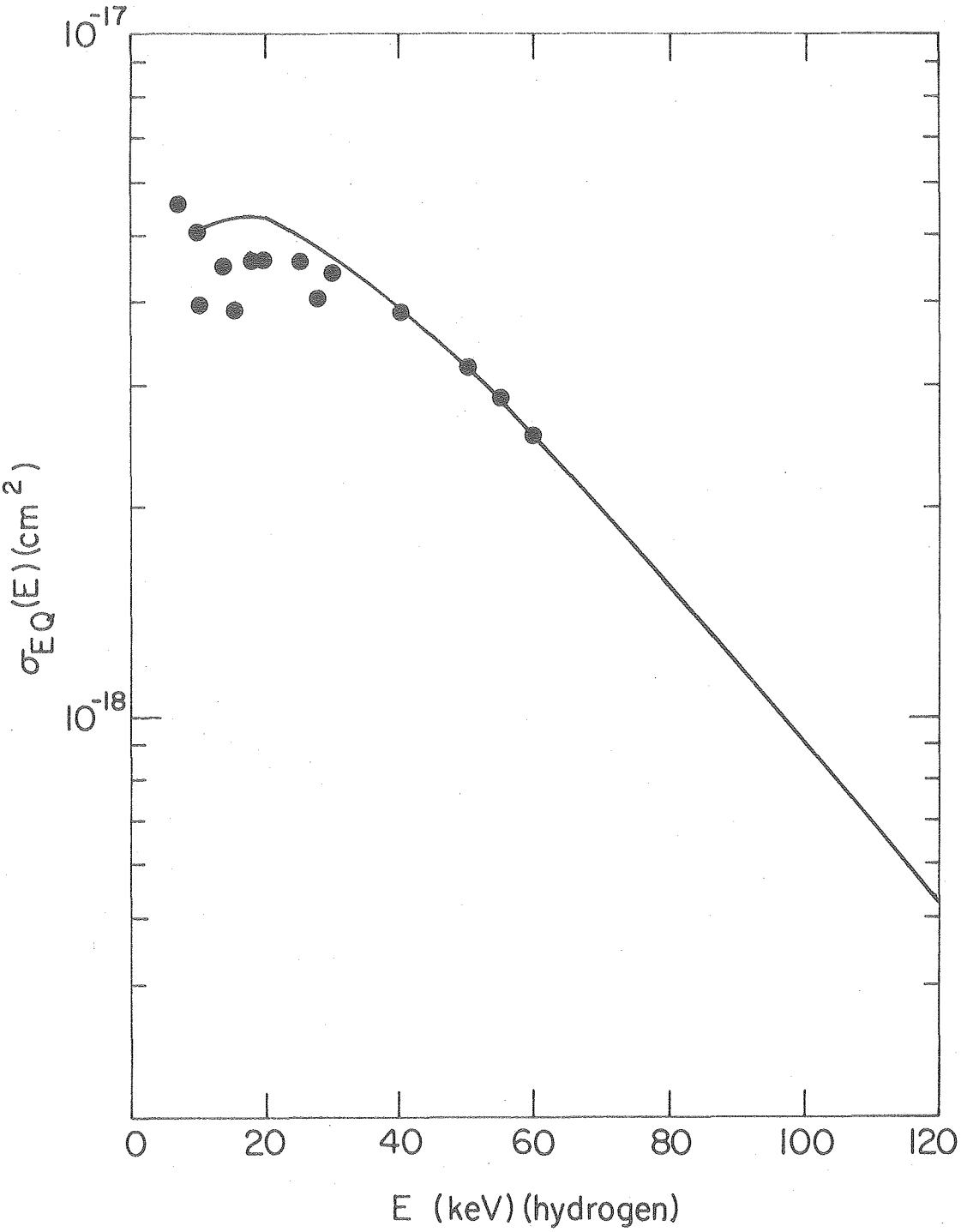

XBL 7912-13388

Fig. 15